Cristofer Jimenez, correspondence author from amt-2018-370 (cristofer.jimenez@tropos.de)

Response to reviews RC1, RC2 and RC3:

On behalf of the authors of the manuscript, I would like to thank the anonymous referees for the constructive feedback given during the first revision of the manuscript. The suggestions and concerns were stated in a clearly and friendly manner, and have been very helpful to reveal writing errors and make the manuscript more comprehensible for readers. Each referee have also expressed concerns and suggestions regarding the presentation of the formalism and results and also about the discussion provided in the manuscript. The comments have been taken carefully into consideration and we have prepared an Answer document in order to address the specific comments of the three reviews RC1, RC2 and RC3.

We kindly invite the editor and reviewers to have a look into the corrected version of the manuscript, which is presented below this answer document. The changes done in response to the reviews have been highlighted with color in the corrected version of the manuscript. Three different colors were used, one for each review: RC1, RC2 and RC3.

Answer to specific comments of RC1:

1. Page 3, Line 9: "…consists of 2''achromatic lens…". Consider providing in a parenthesis also the equivalent of the 2'' in units of mm. **DONE**

2. Page 3, Line 13: Is the value of 650 m theoretically calculated or experimentally measured? In any case consider providing a reference at this point.

   RC1.2 The full overlap altitude was estimated theoretically, the corresponding reference was already on the reference list but not cited on the text. This has been corrected.

3. Page 5, Line 26: Maybe "described" is more appropriate than "considered".

   RC1.3: Yes, I agree with this… DONE

4. Figure 3: Consider annotating this figure with the letters (a), (b), (c), (d), in accordance to the figure legend. Moreover, make clear also in the figure that (a) and (b) refer to the emission while (c) and (d) to the receiving units. **DONE**
5. Page 7, Line 13: "…for the calibration is to insert an additional polarization…" **DONE**
6. Page 7, Line 21: "…, Müller matrices representing…" **DONE**
7. Page 7, Line 27: "P_o is the number of emitted laser photons…" **DONE**
8. Page 8, Line 6: Consider replacing the sub scripts with capital characters, in order to be consistent with the annotation followed in the manuscript. **DONE**
9. Page 9, Line 12: "…, but depends on the receiver…" **DONE**
10. Page 10, Line 14: Eq. 38 is the product of Eq. 25 divided by Eq. 24, and not the inverse. **DONE**
11. In Eq. 42 I am missing the information of the variable C. Please specify to which quantity C refers to.

    <u>RC1.11</u> The interchannel constant X_δ use to be denoted by C. This equation was unintentionally skipped during the change of name from C to X_δ. The authors apologize for this mistake that may have generated confusion during the 1st revision.
12. Page 11, Line 20: "… provides an overview of …" **DONE**
13. Page 11, Line 21: "(above ground level)" **DONE**
14. Consider presenting clearer the x-label of Figure 6 (e.g. $\eta_{tot} \,/\, [\eta_{\parallel,P} \cdot (1 + \varepsilon_r)]$) **DONE**
15. I would kindly suggest to the authors to show the profiles presented in Figure 7 up to higher altitudes (e.g. 4 km). Moreover, the profiles obtained by the ratio $N_P \,/\, N_{tot}$, compared to the rest two, seems to demonstrate greater variability with atmospheric height, in a way that I would say artificial layers are introduced. This can be seen for atmospheric heights inside the water cloud but also below (2.4 - 2.7 km). Is this also a result of the low SNR, even though that the profiles refer to 3 hours of measurement period? In any case the authors are kindly requested to comment on this.

    <u>RC1.15:</u> A second figure has been prepared for the corrected version of the manuscript. As this comment suggests, the profiles obtained with the ratio $N_P \,/\, N_{tot}$ present large variability on the low SNR region, which in our measurements seems more notorious, considering the large attenuation of the 3 channels (to avoid detector saturation at low level clouds). The points considered for the calibrations are however the altitudes where the depolarization is changing, which in clouds is also where the signal strength is large enough for been masked by signal noise. We have commented on this topic in the corrected version of the manuscript.

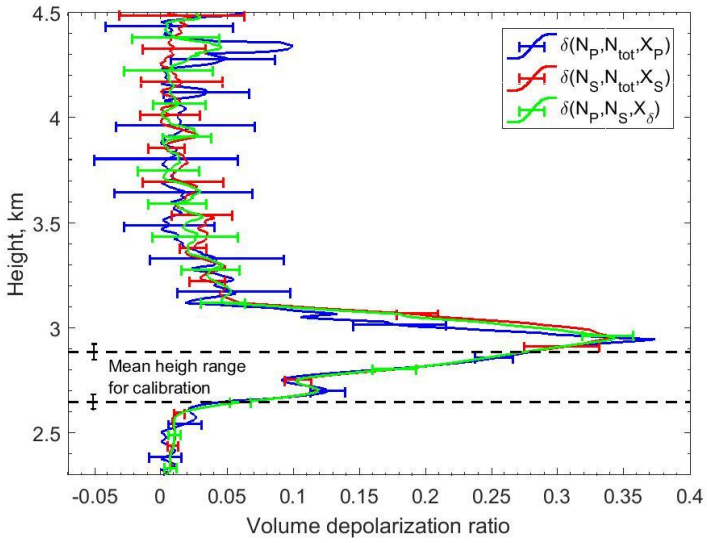

16. Figure 9 is very important. Legend: My suggestion is to use the phrase "(extended 3-signal method)". Additionally, it would be beneficiary for the manuscript if in the same figure, the profile of volume depolarization obtained by the conventional 3-signal technique (Reichard et al., 2003), is also shown. This will clearly demonstrate the improvement achieved by following the extended method proposed here, which takes into account various types of instrumental effects (e.g. the not perfectly polarized emitted laser light).

RC1.16: One of the motivation to develop a new 3-signal approach was that the so called efficiencies ratios D_i ($i = P, S, tot$) has to be known to apply the conventional 3-signal calibration (Reichardt et al., 2003). In the extended 3-signal approach this constants remain unknown. Later on the formulation they are combined with the effect of the angular misalignment between emitter and receiver and with the elliptically polarized laser beam into the global constant ξ_{tot} (in the case of a quasy-ideal system, our case) or into ξ_P and ξ_S (for a non-ideal system).

In principle the 3-signal calibration approach from Reichardt et al. could be implemented, but only after applying our extended calibration approach and knowing the value of ξ_{tot} (required for the calibration). We could add this profile on the Figure but it won't be a rigorous application of the conventional 3-signal calibration approach. To support the validation of the system and calibration approach, instead we added a second measurement for comparison (please see response RC2.14).

17. The manuscript contains many equations and variables and this may easily confuse a reader. Therefore, I would kindly suggest to the authors to list all the variables used in a table (Appendix section), along with a small phrase describing them.
RC1.17: Thanks for this suggestion. A list of variables has been added on the corrected version of the manuscript as Appendix B.

Answer to specific comments of RC2:

1. Abstract: "A comparison with another polarization lidar" replaced by "A comparison with a second polarization lidar" **DONE**

2. Page 2, Line22-25: Please use the same notation for the sections. Currently we can find "section", "Section", "Sect." **DONE**

3. Section 3.1 starts with the statement that the manuscript follows the "notation and explanations of Freudenthaler (2016)" from AMT. Still in the following description, the authors define the misalignment between the polarization axis of the transmitted light and the copolarized receiver channel as θ - Page 5, Line 25-26: "The misalignment between the polarization axis of the transmitted light and the co-polarized receiver channel (defined by the respective polarization filter in front of the PMT) is characterized by angle θ ...."

   The corresponding parameter in Freudenthaler (2016) should be the "Rotation of the plane of horizontal linear polarisation of the laser around the z axis (laser rotation)" which is relative to the receiving unit reference plane. Since the manuscript refers to a similar study performed by a lidar station from the same research network EARLINET-ACTRIS, I would suggest the authors to use the same notation used in the previous work (α). Keeping the same variable names and notations as used in previous studies will help a

reader familiar with similar studies and encourage the use of standardized variables and parameters.

4. Same comment as above applies for Page 6, Line 17: "The rotated polarization axis is represented in Fig. 3c, and after" and Figure 3 (also Page 8, Line 18).

RC2.3-4: **This sentence can lead to confusion indeed, since in our approach we do not adopt the whole nomenclature used in the mentioned recent studies (Freudenthaler 2016, Bravo-Aranda et al. 2016, Belegante et al. 2018).**

The usage of α to describe the rotation angle was considered initially, but finally we opted for θ, since the greek letter α may be confused with the atmospheric extinction coefficient (commonly represented by α). The extinction is not included expressly on the equations since it does not play any role on the depolarization retrieval, some equations include however the term β, to describe the backscattering coefficient, which would have a completely different physical meaning than α representing the angle. Nevertheless, for the corrected version we have changed θ to α with the notation used in (Freudenthaler 2016) for the cosinus, i.e. $c_{2\alpha} = \cos(2\alpha)$.

5. Page 7, Line 13: "A commonly used method for the calibration is ~~the~~ to insert" **DONE**

6. Page 7, Line 27: "$P0$ is the ~~emitted~~ number of emitted laser photons" **DONE**

7. Page 9, Line 25: This section should be described in more detail and the reasoning behind the use of two altitude heights should be clearly mentioned. Please consider extending this section since it is an important part of the theoretical background required to use the calibration technique used in this study.

RC2.7: (please see RC2.7 & 9)

8. Page 10, Line 3: "we obtained a mean value for X_{p}". Is this really "p" or is this "δ"? **DONE**

RC2.8: Yes, it should be δ

9. Page 10, Line 3-9: "Similarly, evaluation of many values of ..... are used to simultaneously determine the volume depolarization ratio in three different ways.". This section should be described in much more detail. Even if most of the readers are experts in lidar techniques, they are not familiar with the theoretical description and formalism presented in the manuscript. The theory behind this calibration technique is really

valuable since this is one of the few manuscripts dealing with the three channel calibration topic and it is important to provide a complete set of information on the theory. This section must be reconsidered before the manuscript is send for publication. **DONE**

RC2.7 & 9: These comments have been taken carefully into consideration, since they reveal important weak points in the description of the method. The content in Page9, line 25 to page 10, line 8 has been reformulated in the corrected version of the manuscript.

The proposed change to the paragraphs from Page 10, line 3-9 is:

"In the conventional 3-signal calibration approach, each signal is normalized to a reference altitude, by doing so the efficiencies of the three channels $\eta_{II,P}$, $\eta_{\perp,S}$ and η_{tot} cancel themselves from the equations, then the ratios between the three normalized signals are calculated. The retrieval of the volume depolarization ratio is done by solving a system of two equations and two unknowns: the volume depolarization ratio at a reference height $\delta(z_0)$ and the volume depolarization ratio at all heights $\delta(z)$ (Reichardt et al., 2003).

In this extended 3-signal calibration procedure, the signals are not normalized to a reference height z_0, instead, we divide directly the signals, obtaining the ratios R_P, R_S and R_δ, by taking then the difference between two altitudes (and not the ratio) we subtract the crosstalk in the emission and reception (ε_l and ε_r) and the angular misalignment ($c_{2\alpha}$). The difference offers additionally a better performance in terms of error propagation compared to the ratio. In this way, the so called interchannel constants (X_δ, X_S and X_P) remain in the equations and they can be estimated by evaluating Eqs. (35), (36) and (37) respectively. Although we can estimate this three constants, we have to note that the number of unknowns are actually two X_P and X_S being the third constant X_δ the ratio of them (please see Eq. (30)), i.e. Eq.(35) is equivalent to Eq.(36) divided Eq. (37).

Given the form of Eqs. (35)-(37), observable differences between the height points z_j and z_k are needed for its evaluation, in practice, only altitude regions should be selected in the determination of X_P, X_S, and X_δ where significant changes in the depolarization ratio occur, e.g., in liquid-water clouds where multiple scattering by droplets produce steadily increasing depolarization with increasing penetration of laser light into the cloud (Donovan et al., 2015; Jimenez et al., 2017; Jimenez et al., 2018). Long measurements periods should be considered for the evaluation of Eqs. (35)-(37). All pair of data points (z_j and z_k in a certain height range, defined according to the ratio of signals) in all single measurements (in time t) provide an array with many observations of the interchannel constants, averaging these arrays we obtain a trustworthy estimate of these constants for the retrieval of the volume depolarization ratio (please see Figure 6)."

10. Page 10, Line 14: "To derive ~~now~~ the linear depolarization" **DONE**

11. Page 10, Line 28: "In the first step, the inter-channel constant X_δ has to be measured." More detail must be provided by the authors. The experimental technique on how to perform the assessment of X_δ must be provided since this is one of the key parameters for the calibration of the depolarization channels.

    RC2.11: We have modified this line in order to give more detail about the technique, since the constant X_δ has to be retrieved, not be measured directly. As change for Page 10, line 8 we propose:
    "As first step of the calibration, the inter-channel constant X_δ (together with X_P and X_S) is obtained from the measurements by evaluating Eqs. (35)-(37) in the selected height range (with variations on the depolarization) at each measurement time t."

12. Eq. 42: please give more details on the missing variable "C".

RC2.12 (same as RC1.11): The interchannel constant X_δ use to be denoted by C. This equation was unintentionally skipped during the change of name from C to X_δ. The authors apologize for this mistake that may have generated confusion during the 1st revision.

13. Page 13, Line 8: "By using constant X_δ and Eq. (42), a mean value of ..." Please provide more information on this topic.

    RC2.13: To provide more information we propose to change the sentence to:
    Using the constant X_δ and evaluating Eq. (42) in the particle-free region of the 3-hour measurement period, a mean value of $\xi_{tot} = 1.118 \pm 0.008$ for the total crosstalk was obtained.

14. Page 14, Line 10-15: Since the comparison between the volume linear depolarization ratio measured by MARTHA and BERTHA is designed to validate the calibration technique used in this study, I would advise to also use a second case for this comparison. A strong depolarizing layer (e.g mineral) would help validate the results for highly depolarizing layers.

    RC2.14: To support the comparative validation. A second simultaneous measurement case was considered for comparison. Page 14 lines 10-15 and Figure 9 have been updated as follows:

To validate the new system and the calibration procedure a comparison between the measurements of the volume linear depolarization ratio with the lidar systems MARTHA and BERTHA (Backscatter Extinction Lidar Ratio Temperature and Humidity profiling Apparatus) is presented in Figure 9. The observations were conducted at Leipzig (51°N, 12°E) on 29 May 2017 with the presence of a Dust layer between 2 and 5 km and a cirrus cloud at 11 km (see Fig. 9a). Good agreement in the dust layer can be noted, while the cirrus cloud shows differences between the two systems, that difference can be attributed to the fact that the BERTHA system is pointing 5° respect to the zenith, while the MARTHA system points to the Zenith (0°). This could lead to specular reflection by horizontally oriented ice crystals reducing the depolarization ratio in the case of the MARTHA system.

A second measurement period during an unique event with a dense biomass burning smoke layer in the stratosphere on 22 August 2017 was considered for comparison (Haarig et al., 2018), here very good agreement for the layer between 5 and 7 km and also for the layer at 14 km was obtained, confirming the good performance of the systems and of the respective calibration procedures, extended 3-signal method in MARTHA and the $\Delta 90°$ method in the BERTHA system.

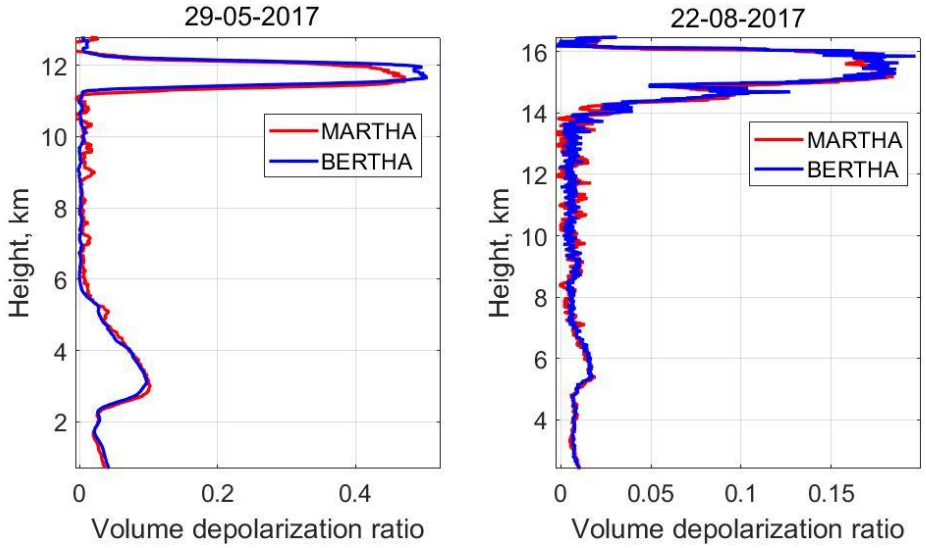

Figure 9: Volume linear depolarization ratio obtained with MARTHA (extended 3-signal method) and BERTHA ($\Delta 90°$ method) on (a) 29 May 2017 20:20-20:45 (with smooth 27 bins) (b) 22 August 2017 20:45-23:15 (Haarig et al., 2018). **The system were located at a distance of 80 meters and were calibrated independently.**

15. Page 17, Line 22-25: I do not see the necessity of this section. A link with further studies was already included in the introduction of the study and since this section is

not connected to the conclusions I would advise to remove it for the final version of the manuscript. **DONE**

16. Since the manuscript has an important theoretical section containing many variables and equations, I would suggest adding an additional list of variables containing a comprehensive description for each element. Please consider following the same terminology used by Freudenthaler (2016) .

RC2.16: Thanks for this suggestion. A list of variables has been added on the corrected version of the manuscript as Appendix B.

Answer to specific comments of RC3

1. Page 4, line 3: *'In the alignment process, the cross-polarized axis is found when the count rates are at the minimum.'*

This process seems to be inaccurate because the change of the signal due to several degrees can be masked by the signal noise. Did you check the accuracy of this procedure? Could you provide the uncertainty?

RC3.1: To find the minimum in the channels P and S we reduce their attenuation (Figure 2) in order to increase the signal strength as much as possible and so avoid noisy signals. The process is still a little bit rudimentary, since the minimum is found by eye rotating manually the mounted filter on the top of the telescopes P and S, so the uncertainty inherent to this aligning process cannot be reported. Therefore, the angular misalignment of the P and S channels with their respective component axis $II\ and\ \perp$ was considered on a first stage as unknown. After applying the new 3-signal calibration procedure, the overall impact on the channels P and S of this angular misalignments, added to the crosstalks of the emission and reception units (ξ_{tot} or ξ_P and ξ_S) can be estimated.

2. Page 4, line 18: *'Based on this theoretical framework we will derive three lidar equations for our three measured signal components.'*

I think that the theoretical framework has not been presented yet. Please, considered to change by 'Based on the theoretical framework of ___, we will derive […]'.

<u>RC3.2:</u> Indeed. We propose the change for Page 4, line 18*:*

"As first step in this theoretical framework, we will derive…"

3. Page 5, lines 10-14: *'In our approach, …'*

I recommend to mention the Figure 3 somehow. It will be easier to understand this paragraph following the steps of Figure 3.

<u>RC3.3:</u> Thanks for this suggestion. An indication of the figure has been added in parenthesis on the manuscript.

4. Page 5, line 18: *'We introduce the so-called crosstalk term $\mathcal{E}_i$'*

In the line 1 of the same page, it is stated that the notation and explanations of previous manuscripts are used. However, the term 'cross-talk' is mainly used to describe non-ideal beamsplitter cubes instead of the depolarization of the outgoing laser light (emitting block). If I properly understood, the cross-talk term would correspond to the depolarisation of the laser light after crossing the transmission block (a king of linear polarisation parameter a_L, according to the Freudenthaler's paper). Additionally, I would say that the angle θ in this manuscript corresponds to the angle α in the Freudenthaler's paper. For the sake of clarity, it would be very helpful for the community whether the same nomenclature is used or, at least, a small mention about the connections is included.

<u>RC3.4</u>: I agree that this sentence can lead to confusion, since in our approach we do not adopt the whole nomenclature used in the mentioned recent studies (Freudenthaler 2016, Bravo-Aranda et al. 2016, Belegante et al. 2018).

The usage of α to describe the rotation angle was considered initially, but finally we opted for θ, since the greek letter α may be confused with the atmospheric extinction coefficient (commonly represented by α). The extinction is not included expressly on the equations since it does not play any role on the depolarization retrieval, some equations include however the term β to describe the backscattering coefficient, which would have a completely different

physical meaning than α representing the angle. Nevertheless, for the corrected version we changed θ to α with the notation used in (Freudenthaler 2016) for the cosines, i.e. $c_{2\alpha} = \cos(2\alpha)$.

The crosstalk of the emission ε_l indicates the depolarization of the light after the transmission block, which would be similar to the linear polarization parameter a_l, adopted in Freudenthaler (2016), but in terms of depolarization.

In the manuscript the term crosstalk is intended to describe the undesirable component on the respective polarization axis, which is assumed to be present during the emission and reception of the wave fronts. In this sense, crosstalk would also hold for the non-ideal response of polarizing beamsplitters.

5. Page 6, line 2 and Eq (6):

According to the Freudenthaler's paper, the rotation R(θ) proposed in this manuscript is a particular case of the emitting block, being other polarizing effects omitted such as the diattenuation. It would be helpful for the readers to have a list of parameters considered ideals.

<u>RC3.5:</u> In the approach further polarizing effects, such as diattenuation and retardation are assumed as ideals, in the emission, characterized by the elliptical polarized wave-front, and also in the reception, where the polarization state of the light is filtered at the beginning of the optical path. Now in Appendix B, indication the parameters assumed as ideals, can be found.

6. Page 6, Figure 3:

It would be helpful for future readers to link each step in the figure with the term, as follow:

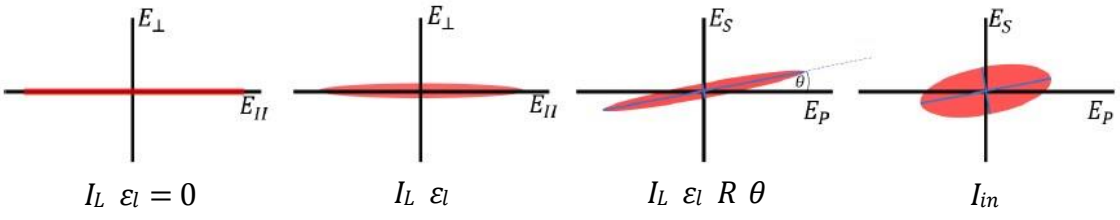

RC3.6: Thanks for this suggestion. It has been implemented on the manuscript. The scheme is much more illustrative now.

7. Page 7, line 13: *'A commonly used method for the calibration is the to insert an extra polarization filter[…]'* **DONE**

Typo? **RC 3.7: Yes**

8. Page 8, line 6: *'Because identical polarization filters are used in our lidar setup, we can assume* $D_P = D_S^{-1}$*.'*

What do you mean with 'identical'? Even the same model of polarizer made by the same company might show quite different behaviors. Additional details should be addressed to support this sentence.

RC3.8: With identical we meant the same filter model. Although the filters may present different extinction ratio, in our approach the difference between D_P and D_S^{-1} are considered as neglectable, since their value should be less than 10^{-3} for 532 nm (according to the fabricant).

Considering the mean value of total crosstalk obtained from the measurements of 2017 ($\xi_{tot} = 1.109 \pm 0.009$), it seems that the parameters that really have an impact on the system (in terms of polarization) are the rotation of the polarization plane θ (now α) and the crosstalk from the emitted laser (ε_l), given the form of this parameter (Eq. (39) on the manuscript).

$$\xi_{tot} = \frac{(1+\varepsilon_r)(1+\varepsilon_l)}{(1-\varepsilon_l)(1-\varepsilon_r)\cos(2\theta)} \geq 1, \quad (39)$$

At the end, the manuscript propose two calibration methods. 1) For a quasy-ideal system ($D_P = D_S^{-1}$ and $\theta_P = \theta_S$, our case) and for a non-ideal system ($D_P \neq D_S^{-1}$ and $\theta_P \neq \theta_S$) (outlined in Appendix A). Lidar users should estimate which approach represent more accurately their system.

We propose to modify Page 8, line 6 to:

"The absence of optical elements before the polarization filters (such as the telescope and beamsplitters) avoids further polarization effects, such as diattenuation and retardation (Freudenthaler, 2016). Moreover, since we employed the same filter model in the optical path of the channels P and S, we assumed that $D_P = D_S^{-1}$*."*

9. Page 9, line 2: *' […] based on a measurement example, we demonstrated that the impact of this assumption can be neglected in our system.'*

Could you provide any indication about the validity of this assumption in other systems?

<u>RC 3.9:</u> Up to now, the only system in our facilities with the three signal implemented is the MARTHA system, therefore the validity of this assumption can only be supported by the results obtained with it.

10. Page 10, line 11: *'liquid-water clouds where multiple scattering by droplets produce steadily increasing depolarization with increasing penetration of laser light into the cloud […]'* and Page 17, line 21: *'the volume of the depolarization ratio does not depend on the field of view of the receiver, however in multiple scattering regime (e.g. in liquid water clouds), it does […]'*.

Could the multiple scattering be a problem for the depolarization calibration?

<u>RC 3.10:</u> The multiple scattering on water droplets is what produce depolarization and does not represent a problem to the calibration (excepting the fact that multiple scattering may increase the signal strength to saturation levels, if the attenuation of the channels is not large enough). The first sentence (Page 10, line 11) aims to indicate that the profile of depolarization in the cloud offers a wide range of values to retrieve the interchannel constants (based on the difference of signal ratios among different heights). The second sentence (Page 17, line 21) is written to indicate that the dependence on the FOV size permits us to assess cloud microphysics by means of depolarization at two or more FOVs. As suggested by the 2nd Review (RC2.15), this sentence will be removed since the link with further studies is already included in the introduction.

11. Page 10, line 29: '*Then ξtot can be estimated in a region (defined by height $zmol$) with dominating Rayleigh backscattering […]*'

This the most important handicap I detect in this method. ξtot must be estimated in a particlefree region where the SNR used to be quite low. This is the same handicap of the classical molecular calibration, including a more complicate ldiar system since three channels are required instead of two. So, why is this method more advisable?

The main difference between with the classical molecular calibration method is that in this approach the molecular region is used to estimate the so called total crosstalk parameter (ξtot). This constant summarizes the impact of the considered systematic error sources (crosstalk in the emission (ε_l) and reception (ε_r) path and angular misalignment between emission and reception ($\cos(2\theta)$ now denoted as $c_{2\alpha}$), and it is expected to be constant with time. On the other hand, the so called interchannel constants (X_P, X_S and X_δ) describe the ratio between the efficiencies of the 3 channels P,S and *tot* to their respective components ($\parallel$, $\perp$ and $\parallel + \perp$) , these efficiencies ($\eta_{II,P}, \eta_{\perp,S}$ and η_{tot}) represent the product of the effective area of the receiver, the transmissivity of the optical path (modulated by the attenuation setup) and also the gain and efficiency of the detectors, These constants (X_P, X_S and X_δ) are expected to vary with time, as the attenuation is eventually change by users, and also as the efficiency of the detectors decays with time.

This method would be more advisable since it separates the unknowns of the problem in constants that vary with time (X_P, X_S and X_δ) and a constant that does not change with time (ξtot) estimated in the particle-free region. When averaging long term measurements, we can get rid of the eventual bias induced by aerosol particles present in the region considered as free-particle region, allowing an accurate estimate of this non-changing constant.

12. Page 11, Eq. (42):

Which is the meaning of the term 'C'? I was not able to find its definition. From Eq. (41) to Eq.

(42), I got that $C = X_\delta$. Please, specify it.

<u>RC3.12 (same as RC1.11 & RC2.12):</u> The interchannel constant X_δ use to be denoted by C. This equation was unintentionally skipped during the change of name from C to X_δ. The authors apologize for this mistake that may have generated confusion during the 1st revision.

13. Page 12, line 10 and caption of Figure 6:

Whereas it is stated that the height range goes from a few meters below the cloud base up to 240 m above (page 12 line 10) in the caption of the Figure 6, it is noted that 16000 data points were obtained. Could you explain the huge number of data points in this small height range?

RC3.13: **For the calculations of the calibration constants, each pair of bins in the 240 meters are considered for the evaluation of Eqs. (35)-(37). In a 5 minutes profile we get one result at each combination of height bins in the selected range, for 32 height bins (240 meters), we get $\sum_{n=1}^{31} n = 496$ combinations. Considering all the 5-min profiles in the hours of measurement we get actually 17856 data points. The Figure label has been corrected to the right amount of points (about 18000).**

14. Page 13, line 8: *'The crosstalk factor has a large impact on the retrieval of the volume linear depolarization ratio only in the region with low depolarization ratios.'*

Please, include whatever is necessary to demonstrate this sentence.

RC3.14: We have reformulated this sentence to make clearer the point. We changed the Page 13, line 8 to:

"Given the form of the equations to retrieve the profiles of volume depolarization ratio (Eqs. (35)-(37)), the propagated uncertainty associated to ξ_{tot} does not vary largely with height, which leads to a large percentage uncertainty on the retrieval of the volume linear depolarization ratio in the region with low depolarization ratios, also characterized by low signal strengths"

15. Page 15, line 8: *'4.2 Long-term stability of the polarization lidar calibration and performance'* and Page 17, line 18: *'Long term studies indicated the robustness and stability of the three-signal lidar system over long time periods.'*

The calibration stability was analyzed between April and November 2017 (8 months). I would use 'long-term' for larger periods and thus, I suggest replacing 'long-term stability' by 'temporal stability'. **DONE**

16. Page 15, line 15: *'The selected large attenuation of the channels prohibited an optimum detection of high-level dust layers and ice clouds.'*

Could you explain how the large attenuation prohibited an optimum detection of dust layers but allowed the determination of ξtot using the molecular depolarization ratio?

RC3.16: **It is meant that on this layer, the determination of the interchannel constants is not optimal, since it requires the differences of the signal ratios between single height bins. The large attenuation on the channels for this system (since this system particular aims to measure depolarization in liquid clouds) reduce the SNR in aerosol layers making difficult to use the mentioned difference of ratios. For the estimation of ξtot, we can average the whole measurement period and a large height range reducing considerably the impact of the noise of the measurements.**

We have changed this sentence to:

"One reason for these differences in the uncertainty of X_δ is that the system was optimized for the observation of low-altitude liquid-water clouds, for which the detection channels need large attenuation to avoid saturation of the detectors in the cloud layer. This setup prohibited an optimum detection of high-level dust layers and ice clouds due to the low signal strength for these cases."

17. Page 15, line 15:

Typo: double space 'can be__noted'. **DONE**

18. Page 17, line 2: *'based on three telescopes with a polarization filter on the front'.*

Do authors mean three 'channels'?

RC3.18: **We meant telescopes indeed. We propose the change on the text:** *"based on three telescopes (one for each channel) with a polarization filter on the front"*

19. Page 17, line 13: *'However, it needs a strong depolarizing medium for its application, e.g., water clouds.'*

This phrase might be confusing. Please, clarify that the strong depolarization comes from the multiple scattering not because the liquid droplets.

RC3.19: **This can be confusing indeed. To avoid confusion with this sentence, we propose to change it to:**

"However, it needs a strong depolarizing medium for its application, such as dust layers and also water clouds, which depolarize the light due to multiple scattering in droplets or due to single scattering of ice particles"

Polarization lidar: An extended three-signal calibration approach

Cristofer Jimenez[1], Albert Ansmann[1], Ronny Engelmann[1], Moritz Haarig[1], Jörg Schmidt[2], and Ulla Wandinger[1]

[1]Leibniz Institute for Tropospheric Research, Leipzig, D-04318, Germany

[2]University of Leipzig, Institute for Meteorology, Leipzig, D-04103, Germany

Correspondence to: Cristofer Jimenez (cristofer.jimenez@tropos.de)

Abstract. We present a new formalism to calibrate a three-signal polarization lidar and to measure highly accurate height profiles of the volume linear depolarization ratios under realistic experimental conditions. The methodology considers elliptically polarized laser light, angular misalignment of the receiver unit with respect to the main polarization plane of the laser pulses, and crosstalk between the receiver channels. A case study of a liquid-water cloud observation demonstrates the potential of the new technique. Long-term observations of the calibration parameters corroborate the robustness of the method and the long-term stability of the three-signal polarization lidar. A comparison with a second polarization lidar shows excellent agreement regarding the derived volume linear polarization ratios in different scenarios: a biomass burning smoke event throughout the troposphere and the lower stratosphere up to 16 km height, a dust case and also a cirrus cloud case.

1 Introduction

Atmospheric aerosol particles influence the evolution of clouds and the formation of precipitation in complex and not well understood ways. Strong efforts are needed to improve our knowledge about aerosol-cloud interaction and the parameterization of cloud processes in atmospheric (weather and climate) models, weather forecasts, and especially to decrease the large uncertainties in future climate predictions (IPCC 2013). Besides more measurements in contrasting environments with different climatic and air pollution conditions, new experimental (profiling) methods need to be developed to allow an improved and more direct observation of the impact of different aerosol types and mixtures on the evolution of liquid-water, mixed-phase, and ice clouds occurring in the height range from the upper planetary boundary layer to the tropopause. Active remote sensing is a powerful technique to continuously and coherently monitor the evolution and life cycle of clouds in their natural environment.

Recently, Schmidt et al. (2013, 2014, 2015) introduced the so-called dual-field-of-view (dual-FOV) Raman lidar technique which allows us to measure aerosol particle extinction coefficients (used as aerosol proxy) close to cloud base of a liquid-water cloud layer and to retrieve, at the same time, cloud microphysical properties such as cloud droplet effective radius and cloud droplet number concentration (CDNC) in the lower part of the cloud layer. In this way, the most direct impact of aerosol particles on cloud microphysical properties could be determined. However, the method is only applicable after sun set (during nighttime) and signal averaging of the order of 10-30 minutes is required to reduce the impact of signal noise on the observations to a tolerable level. As a consequence, cloud properties cannot be resolved on scales of 100-200 m horizontal

resolution or 10-30 s. To improve the dual-FOV measurement concept towards daytime observations and shorter signal averaging times (towards time scales allowing us to resolve individual, single updrafts and downdrafts) we developed the so-called dual-FOV polarization lidar method (Jimenez et al., 2017, 2018a). This technique makes use of strong depolarization of transmitted linearly polarized laser pulses in water clouds by multiple scattering of laser photons by water droplets (with typical number concentrations of 100 cm^{-3}). This novel polarization lidar method can be applied to daytime observations with resolutions of 10-30 s. An extended description of the method is in preparation (Jimenez et al., 2018b).

Highly accurate observations of the volume linear depolarization ratio are of fundamental importance for a successful retrieval of cloud microphysical properties by means of the new polarization lidar technique. In this article (part 1 of a series of several papers on the dual-FOV polarization lidar technique), we present and discuss our new polarization lidar setup and how the lidar channels are calibrated. The basic product of a polarization lidar is the volume linear depolarization ratio, defined as the ratio of the cross-polarized to the co-polarized atmospheric backscatter intensity, and is derived from lidar observations of the cross and co-polarized signal components, or alternatively, from the observation of the cross-polarized and total (cross + co-polarized) signal components. Cross and co-polarized denote the plane of linear polarization, orthogonal and parallel to the linear polarization plane of the transmitted laser light, respectively. Reichardt et al. (2003) proposed a robust concept to obtain high-quality depolarization ratio profiles by measuring simultaneously three signal components, namely the cross and co-polarized signal components and additionally the total elastic backscatter signal. We will follow this idea as described in Sect. 2. Reichardt et al. (2003) assumed that the laser pulses are totally linearly polarized. Recent studies, however, have shown that the transmitted laser pulses can be slightly elliptically polarized (David et al., 2012; Freudenthaler, 2016; Bravo-Aranda et al., 2016; Belegante et al., 2018). We will consider this effect in our extended approach of the three-channel depolarization technique. We further extend the formalism by considering realistic strengths of crosstalk between the three channels and we propose a practical inversion scheme based on the determination of the instrumental constants for the retrieval of high temporal resolution volume depolarization ratio profiles.

The article is organized as follows. In Sect. 2, the lidar instrument is described. The new methodology to calibrate the lidar system and to obtain high quality depolarization ratio observations is outlined in Sect. 3. Sect. 4 presents and discusses atmospheric measurements performed to check and test the applicability of the new methodology. Concluding remarks are given in Sect. 5.

2 Lidar setup

A sketch of the instrumental setup, providing an overview of the entire lidar system, is shown in Fig. 1. MARTHA (Multiwavelength Tropospheric Raman lidar for Temperature, Humidity, and Aerosol profiling) has a powerful laser transmitting in total 1~J per pulse at a repetition rate of 30~Hz and has an 80~cm telescope, and is thus well designed for tropospheric and stratospheric aerosol observations (Mattis et al., 2004, 2008, 2010; Schmidt et al., 2013, 2014, 2015; Jimenez

et al., 2017, 2018). MARTHA belongs to the European Aerosol Research Lidar Network (EARLINET) (Pappalardo et al., 2014). We implemented a new three-signal polarization lidar receiver unit to the left side of the large telescope (see Fig. 1). The new receiver setup is composed of three independent telescopes co-aligned with the lidar transmitter.

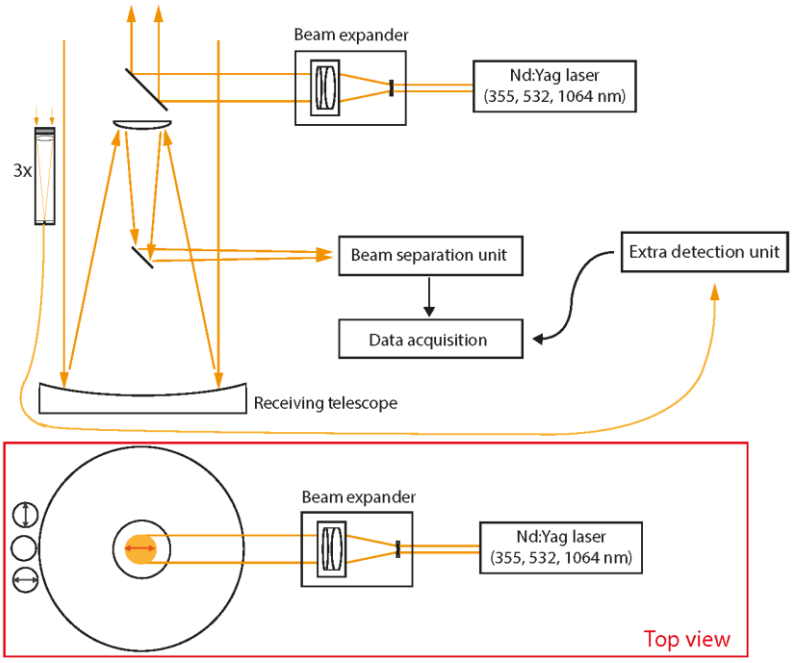

Figure 1: Overview of the EARLINET lidar MARTHA. The three-signal receiver unit of the new polarization lidar setup (details are shown in Fig. 2) is integrated into the MARTHA telescope construction (left side in both of the two sketches). The outgoing laser beam is 54 cm away from the new polarization-sensitive receiver unit. The main plane of linear polarization of the laser pulses and the polarization sensitivity of cross- and co-polarized receiver channels are indicated by arrows in the top-view sketch.

Figure 2 provides details of the new polarization-sensitive channels. Each of the small receiver telescopes consist of 2" (50.8 mm) achromatic lens with a focal length of 250 mm. An optical fiber with an aperture of 400 µm is placed at the focal point of the lens. The resulting field of view (FOV) is 1.6 mrad. The receivers have in principle the same overlap function, since they are identical and are implemented into the large telescope at the same distance from the laser beam axis. The laser-beam receiver-FOV overlap (obtained theoretically) is complete at about 650 m above the lidar (Stelmaszczyk et al., 2005).

At the output of the fiber a 2 mm ball lens is placed (scrambler in Fig. 2) in order to remove the small sensitivity of the interference filter to the changing incidence angle of backscattered light in the near-range. Only above 650 m (full overlap), we can assume that all light from all heights is backscattered at exactly 180°. A spatial attenuation unit which consists of two optical fibers is integrated in the receiver setup, replacing the usual setup with neutral density filters. The distance between the

two fibers with given aperture can be changed and thus the strength of the incoming lidar return signal. The attenuation factor depends on the square of the distance between the fibers and on the numerical aperture of the fibers. E.g., signal attenuation by a factor of about 100 when the distance is 25 mm, and about 1000 with 79 mm distance.

The purpose of the new receiver system is to measure accurate profiles of the volume depolarization ratio in clouds between 1 and 12 km height. For the separation of the polarization components two of the three polarization telescopes are equipped with a linear polarization filter (see Fig. 2, linear polarizer) in front of the entrance lens. In the alignment process, the cross-polarized axis is found when the count rates are at the minimum. The co-polarized channel is then rotated by 90° compared to the cross-polarized filter position, because it is set manually, the difference between the true polarization axis of the filters may not be 90°, however, in this approach we will assume it, since the impact of small variations in the pointing angles of the polarization filters can be neglected (see Appendix A). Additionally, a small tilt between the finally obtained polarization plane of the receiver unit and the true polarization state (main plane of linear polarization) of the transmitted laser pulses is expected and thus assumed in the methodology outlined in Sect. 3**.**

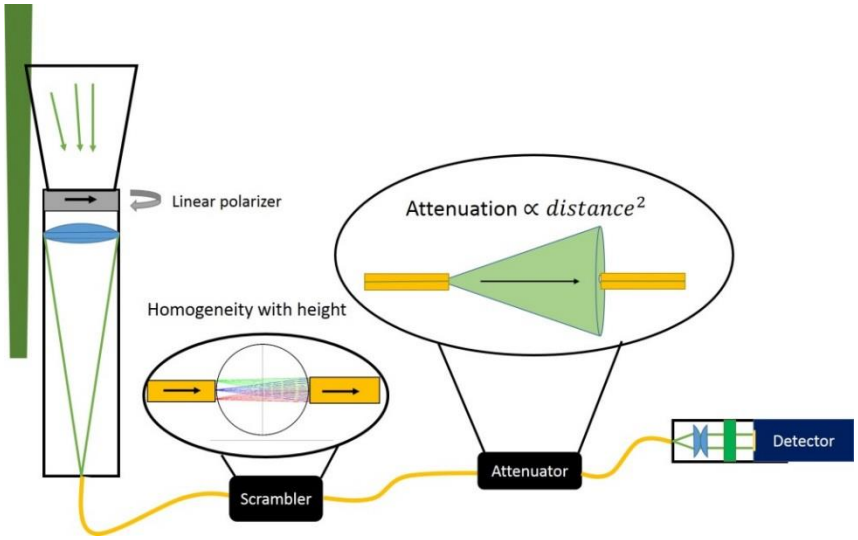

Figure 2: Sketch of one of the three identical receiver channel of the three-signal polarization lidar. The different parts are explained in the text.

3 Methodology

In Sect. 3.1, we begin with definitions and equations that allow us to describe the transmission of polarized laser pulses into the atmosphere, backscatter, extinction, and depolarization of polarized laser radiation by the atmospheric constituents, and the influence of the receiver set up on the depolarization ratio measurements. As first step in this theoretical framework we

will derive three lidar equations for our three measured signal components. In Sect. 3.2, we then present the derivation of the new three-signal method for the determination of the volume depolarization ratio starting from the three lidar equations (one for each channel) defined in Sect. 3.1.

3.1 Theoretical background: Three-signal polarization lidar

We follow the explanations and part of the notation of Freudenthaler (2016), Bravo-Aranda et al. (2016), and Belegante et al. (2018) in the description of the lidar setup, from the laser source (as part of the transmitter unit) to the detector unit (as part of the receiver block), and regarding the interaction of the polarized laser light photons with atmospheric particles and molecules by means of the Müller- Stokes formalism (Chipman, 2009). A Stokes vector describes the flux and the state of polarization of the transmitted laser radiation pulses and Müller matrices describe how the optical elements of the transmitter and receiver units and the atmospheric constituents change the Stokes vector. The laser beam is expanded before transmission into the atmosphere. In most polarization lidar applications it is assumed that the transmitted laser radiation is totally linearly polarized. But this is not the case in practice. In our approach, we therefore take into consideration that the transmitted wave front contains a non-negligible, small amount of cross-polarized light after passing through the beam expander. Additionally, we consider a small-angular misalignment, described by angle α between the main plane of polarization of the laser beam and the orientation of the respective plane of polarization defined by the polarization filters in front of the telescopes of the receiver unit of our three-channel polarization lidar configuration described below (these considerations can be visualized in Fig. 3).

The transmitted radiation $P_0(z)$ of the laser pulse can be written as the sum

$$P_0 = P_{0,II} + P_{0,\perp} \tag{1}$$

with the co- and cross-polarized light components, $P_{0,II}$ and $P_{0,\perp}$, with polarizations parallel and orthogonal to the main plane of laser light polarization. We introduce the so-called crosstalk term ε_l,

$$\varepsilon_l = \frac{P_{0,\perp}}{P_{0,II}}, \tag{2}$$

which describes the small amount of cross-polarized light in the laser beam after leaving the transmission block of the lidar towards the atmosphere. Now we can write:

$$P_0 = (1 + \varepsilon_l)P_{0,II}. \tag{3}$$

The transmitted electromagnetic wave front is then given by the Stokes vector (Lu and Chipman, 2009)

$$\boldsymbol{I_L} = P_{0,II}\begin{pmatrix} 1+\varepsilon_l \\ 1-\varepsilon_l \\ 0 \\ 0 \end{pmatrix} = P_0\begin{pmatrix} 1 \\ \frac{1-\varepsilon_l}{1+\varepsilon_l} \\ 0 \\ 0 \end{pmatrix}. \tag{4}$$

The misalignment between the polarization axis of the transmitted light and the co-polarized receiver channel (defined by the respective polarization filter in front of the PMT) is characterized by angle α and described by the rotation Müller matrix (Bravo-Aranda et al., 2016), here we adopt the notation for the trigonometric functions used in (Freudenthaler, 2016), i.e., $\cos(2\alpha) := c_{2\alpha}$ and $\sin(2\alpha) := s_{2\alpha}$:

$$\mathbf{R}(\boldsymbol{\alpha}) = \begin{pmatrix} 1 & 0 & 0 & 0 \\ 0 & \cos(2\alpha) & -\sin(2\alpha) & 0 \\ 0 & \sin(2\alpha) & \cos(2\alpha) & 0 \\ 0 & 0 & 0 & 1 \end{pmatrix} = \begin{pmatrix} 1 & 0 & 0 & 0 \\ 0 & c_{2\alpha} & -s_{2\alpha} & 0 \\ 0 & s_{2\alpha} & c_{2\alpha} & 0 \\ 0 & 0 & 0 & 1 \end{pmatrix} \quad (5)$$

Then the incident field after backscattering by atmospheric particles and molecules, and before passing the receiver block can be written as (Freudenthaler, 2016):

$$\boldsymbol{I_{in}} = \mathbf{FR}(\boldsymbol{\alpha})\boldsymbol{I_L} = F_{11} \begin{pmatrix} 1 & 0 & 0 & 0 \\ 0 & a & 0 & 0 \\ 0 & 0 & -a & 0 \\ 0 & 0 & 0 & 1-2a \end{pmatrix} \begin{pmatrix} 1 & 0 & 0 & 0 \\ 0 & c_{2\alpha} & -s_{2\alpha} & 0 \\ 0 & s_{2\alpha} & c_{2\alpha} & 0 \\ 0 & 0 & 0 & 1 \end{pmatrix} P_0 \begin{pmatrix} 1 \\ \frac{1-\varepsilon_l}{1+\varepsilon_l} \\ 0 \\ 0 \end{pmatrix},$$

$$\boldsymbol{I_{in}} = F_{11} P_0 \begin{pmatrix} 1 \\ \frac{1-\varepsilon_l}{1+\varepsilon_l} c_{2\alpha} a \\ -\frac{(1-\varepsilon_l)}{1+\varepsilon_l} s_{2\alpha} a \\ 0 \end{pmatrix} \quad (6)$$

with the atmospheric polarization parameter

$$a = \frac{1-\delta}{1+\delta}. \quad (7)$$

The scattering matrix **F** describes the interaction of the laser photons with the atmospheric particles and molecules. F_{11} and δ are the backscatter coefficient and the volume linear depolarization ratio, respectively.

The true volume backscatter coefficient ($\beta := F_{11}$) is given by

$$\beta = \beta_{II} + \beta_{\perp} = (1+\delta)\beta_{II} \quad (8)$$

with the backscatter contributions for the co- and cross-polarization planes (with respect to the true polarization planes given by the transmitted laser pulses). The volume linear depolarization ratio is defined as

$$\delta(z) = \frac{\beta_{\perp}(z)}{\beta_{II}(z)}. \quad (9)$$

Figure 3 illustrates the different polarization states and configurations of the original laser pulses (Fig. 3a) and after leaving the beam expander as elliptically polarized laser light (Fig. 3b). The receiver block may be not well aligned to the main plain of laser radiation so that the PMT measures different cross- and co polarized signal components with respect the outgoing cross- and co-polarized laser light components in Fig. 3b. The rotated polarization axis is represented in Fig. 3c, and after being backscattered and depolarized, the incident polarization plane has the form as shown in Fig. 3d.

To distinguish the apparent, measured volume backscatter coefficient, determined from the actually measured co- and cross-polarized signal components which are related to the incident field $\boldsymbol{I_{in}}$ (Eq. (6), see Fig. 3c) we introduce index 'in' and have the following relationships and links to the (true) laser light polarization plane:

$$\beta_{in} = \beta_{II,in} + \beta_{\perp,in} = \beta, \quad (10)$$

$$\beta_{II,in} - \beta_{\perp,in} = \frac{1-\varepsilon_l}{1+\varepsilon_l} c_{2\alpha} a \beta. \quad (11)$$

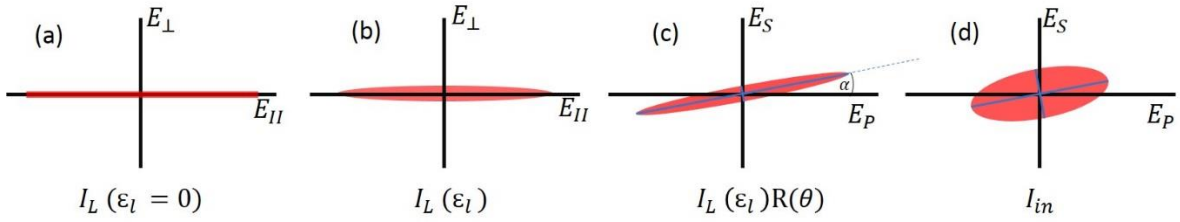

Figure 3: (a) Polarization state of the light generated by the laser (100% linearly polarized), *E* denotes electromagnetic field. (b) The laser radiation is elliptically polarized after passing the beam expander (see Fig. 1). (c) The receiving cross- and co-polarized signal channels (E_S and E_P) are usually not perfectly aligned to the main polarization plane of the laser radiation, i.e. $\alpha > 0$. (d) Polarization plane in the receiver for light which has been backscattered and depolarized by the atmosphere.

Using now Eq. (10) (describing the first term of $\boldsymbol{I_{in}}$ in Eq. (6)) and Eq. (11) (describing the second term of $\boldsymbol{I_{in}}$ in Eq. (6)), the apparent backscatter components $\beta_{II,in}$ and $\beta_{\perp,in}$ can be written as:

$$\beta_{II,in} = \left(1 + \frac{(1-\delta)}{(1+\delta)}\frac{(1-\varepsilon_l)}{(1+\varepsilon_l)}\mathrm{c}_{2\alpha}\right)\beta/2, \tag{12}$$

$$\beta_{\perp,in} = \left(1 - \frac{(1-\delta)}{(1+\delta)}\frac{(1-\varepsilon_l)}{(1+\varepsilon_l)}\,\mathrm{c}_{2\alpha}\right)\beta/2\,. \tag{13}$$

These three backscattering components (Eqs. (10), (12), and (13)) can be measured separately using the three different telescopes of our polarization lidar described in Sect. 2.

It is worthwhile to mention that polarization lidars typically have two detection channels, either a cross-polarized and a parallel-polarized channel or a cross-polarized and so-called total channel. A commonly used method for the calibration is to insert an additional polarization filter into the optical path of the receiver unit and to rotate or tilt a $\lambda/2$ plate (Liu and Wang, 2013; Engelmann et al., 2016, McCullough et al., 2017). For these calibrations an extra measurement period is required. This calibration can introduce new and significant uncertainties (Biele et al., 2000; Freudenthaler et al., 2009; Mattis et al., 2009; Haarig et al., 2017).

As mentioned in the introduction, the concept to calibrate a lidar depolarization receiver by using three channels was proposed by Reichardt et al. 2003. The method consists of an absolute calibration procedure based on the measurement of elastically backscattered light with three detection channels for measuring co-, cross- and totally polarized backscatter components.

To determine the number of counts that the detection channels measure, Müller matrices representing the optical path of each channel would need to be added on Eq. (6). Nevertheless, in this approach we follow the view adopted by Reichardt et al. (2003), where the traditional lidar equation is used to characterize the lidar channels.

Let us now introduce the lidar equations for these three signals. Following Reichardt et al. (2003), the number of photons N_i that a lidar detects at height z (above the full overlap height) with channel i is given by

$$N_i(z) = P_0\left(\eta_{II,i}\beta_{II,in}(z) + \eta_{\perp,i}\beta_{\perp,in}(z)\right)T^2(z)/z^2. \tag{14}$$

P_0 is the number of emitted laser photons and $\eta_{II,i}$ and $\eta_{\perp,i}$ are the optical efficiencies regarding the co- and cross-polarized components ($\beta_{II,in}$ and $\beta_{\perp,in}$) of the backscattered light that arrives at the channel-*i* detector. These efficiencies include instrumental constants that contain the total transmittance through all optical components and gain of the detectors and attenuation in the path of each channel. *T* denotes the atmospheric single-path transmission and is the same for all three detection channels (co, cross and total), since the extinction is independent of the state of polarization of the light. Rearrangements lead to the following versions of the lidar equations for the cross (*S*) and co-polarized (*P*) channels:

$$N_i(z) = P_0\,\eta_{II,i}\left(\beta_{II,in}(z) + D_i\beta_{\perp,in}(z)\right)T^2(z)/z^2, \tag{15}$$

or

$$N_i(z) = P_0\,\eta_{\perp,i}\left(D_i^{-1}\beta_{II,in}(z) + \beta_{\perp,in}(z)\right)T^2(z)/z^2, \tag{16}$$

here D_i denotes the so-called efficiency ratio (Reichardt et al., 2003), and it is defined as:

$$D_i := \frac{\eta_{\perp,i}}{\eta_{II,i}}, \tag{17}$$

The absence of optical elements before the polarization filters (such as the telescope itself and beamsplitters) avoids further polarization effects, such as diattenuation and retardation (Freudenthaler, 2016). Moreover, since we employed the same filter model in the optical path of the channels P and S, we assumed that $D_P = D_S^{-1}$. In the case of the total signal component (*i*= tot*)* we assume that $D_{tot} = 1$ and we introduce the overall efficiency η_{tot} for simplicity reasons. The numbers of photons measured with each of the three channels (*i* = P, S, tot*)* are then given by

$$N_P(z) = P_0\eta_{II,P}\left(\beta_{II,in}(z) + D_P\beta_{\perp,in}(z)\right)T^2(z)/z^2, \tag{18}$$

$$N_S(z) = P_0\eta_{\perp,S}\left(\beta_{\perp,in}(z)+D_S^{-1}\beta_{II,in}(z)\right)T^2(z)/z^2, \tag{19}$$

$$N_{\mathrm{tot}}(z) = P_0\eta_{tot}\beta_{in}(z)T^2(z)/z^2. \tag{20}$$

After further rearranging we finally obtain:

$$\frac{N_P(z)z^2}{\eta_{II,P}P_0T^2(z)} = \beta_{II,in}(z) + D_P\beta_{\perp,in}\,(z), \tag{21}$$

$$\frac{N_S(z)z^2}{\eta_{\perp,S}P_0T^2(z)} = \beta_{\perp,in}(z) + D_S^{-1}\,\beta_{II,in}(z), \tag{22}$$

$$\frac{N_{tot}(z)z^2}{\eta_{\mathrm{tot}}P_0T^2(z)} = \beta_{in}(z). \tag{23}$$

To consider, in the next step, receiver misalignment and crosstalk effects, we introduced the parameters $\mathcal{E}_l = \frac{P_{0,\perp}}{P_{0,II}}$ (Eq. (2)), describing the small amount of cross-polarized light in the laser beam after leaving the transmission block into the atmosphere, and the rotation angle α, describing the angular misalignment between the transmitter and receiver units. To consider also the receiver-channel crosstalk, we further introduce $\mathcal{E}_r$, defined by $\mathcal{E}_r = D_S^{-1} = D_P$. The receiver crosstalk value is typically $\mathcal{E}_r \leq 10^{-3}$ (according to the filter manufacturer) as here the only element to consider is the polarization filter in front of the telescopes. Combining now Eqs. (10), (12), and (13) with Eqs. (21) - (23), we can write:

$$\frac{N_P(z)z^2}{\eta_{II,P}\,P_0T^2(z)} = \beta_{II,in}(z) + \varepsilon_r\beta_{\perp,in}(z) = \left(1 + \varepsilon_r + \frac{(1-\delta(z))}{(1+\delta(z))}\frac{(1-\varepsilon_l)}{(1+\varepsilon_l)}\,(1-\varepsilon_r)c_{2\alpha}\right)\beta(z)/2, \quad (24)$$

$$\frac{N_S(z)z^2}{\eta_{\perp,S}P_0T^2(z)} = \beta_{\perp,in}(z) + \varepsilon_r\,\beta_{II,in}(z) = \left(1 + \varepsilon_r - \frac{(1-\delta(z))}{(1+\delta(z))}\frac{(1-\varepsilon_l)}{(1+\varepsilon_l)}\,(1-\varepsilon_r)c_{2\alpha}\right)\beta(z)/2, \quad (25)$$

$$\frac{N_{tot}(z)z^2}{\eta_{tot}P_0T^2(z)} = \beta_{in}(z) = \beta(z). \quad (26)$$

Until this point, the analytical procedure has been based on the assumption that the polarization filters in front of the cross- and co-polarized telescopes are pointing 90° with respect to each other. However, in the general case, when their angular deviation with respect to their respective components is different (E_P to E_{II} and E_S to $E_\perp$), Eqs. (24) and (25) have a different angular component. In this approach, we keep this assumption for the development of a simple calibration procedure. In Appendix A, the general case is evaluated (angle P to S ≠ 90°), and based on a measurement example, we demonstrated that the impact of this assumption can be neglected in our system.

3.2 Determination of calibration constants and the volume linear depolarization ratio

Outgoing from Eqs. (24)-(26) we will define instrumental (inter-channel) constants which are required to calibrate the lidar in the experimental practice and which are also used in the determination of the volume linear depolarization ratio. The equations for the determination of the depolarization ratios will be given. Three different ways can be used to determine the linear depolarization ratio profiles.

Considering Eq. (26) and the sum of Eqs. (24) and (25), we can write

$$\frac{N_{tot}(z)}{\eta_{tot}} = \frac{1}{1+\varepsilon_r}\left(\frac{N_P(z)}{\eta_{II,P}} + \frac{N_S(z)}{\eta_{\perp,S}}\right), \quad (27)$$

Eq. (27) is independent of the transmission crosstalk factor ε_l and of the rotation of the receiver axis (and thus rotation angle α), but depends on the receiver crosstalk factor ε_r.

Let us introduce the following inter-channel instrumental constants

$$X_P = \frac{\eta_{tot}}{(1+\varepsilon_r)\eta_{II,P}}, \quad (28)$$

$$X_S = \frac{\eta_{tot}}{(1+\varepsilon_r)\eta_{\perp,S}}, \quad (29)$$

$$X_\delta = \frac{\eta_{II,P}}{\eta_{\perp,S}} = \frac{X_S}{X_P} \quad (30)$$

and the signal ratios R_P, R_S, R_δ

$$R_P(z) = {N_P(z)}\Big/{N_{tot}(z)}, \quad (31)$$

$$R_S(z) = {N_S(z)}\Big/{N_{tot}(z)}, \quad (32)$$

$$R_\delta(z) = {N_S(z)}\Big/{N_P(z)}. \quad (33)$$

By using these definitions, Eq. (27) (after multiplication with $\frac{\eta_{tot}}{N_{tot}(z)}$) can be rearranged to

$$X_P R_P(z) + X_S R_S(z) = 1. \quad (34)$$

Eq. (34) is only valid for the case of an almost ideal polarization lidar receiver unit, i.e., when $D_S^{-1} = D_P$ $(= \mathcal{E}_r)$. This is not the case for most of lidar systems where the receiver and separation unit may introduce differences between the transmission ratios D_S^{-1} and D_P. In the next step, we form the difference of Eq. (34) for altitude z_j minus Eq. (34) for altitude z_k and obtain:

$$X_\delta(z_j, z_k, t) = -\frac{R_P(z_j,t) - R_P(z_k,t)}{R_S(z_j,t) - R_S(z_k,t)}, \quad (35)$$

in the same way, when Eq. (27) is multiplied by $\frac{\eta_{\perp,S}}{N_S(z)}$ and $\frac{\eta_{II,P}}{N_P(z)}$, we can derive Eqs. (36) and (37) respectively.

$$X_S(z_j, z_k, t) = \frac{R_P^{-1}(z_j,t) - R_P^{-1}(z_k,t)}{R_\delta(z_j,t) - R_\delta(z_k,t)}, \quad (36)$$

$$X_P(z_j, z_k, t) = \frac{R_S^{-1}(z_j,t) - R_S^{-1}(z_k,t)}{R_\delta^{-1}(z_j,t) - R_\delta^{-1}(z_k,t)} \quad (37)$$

t denotes time.

In the conventional 3-signal calibration approach, each signal is normalized to a reference altitude, by doing so the efficiencies of the three channels $\eta_{II,P}$, $\eta_{\perp,S}$ and η_{tot} cancel themselves from the equations, then the ratios between the three normalized signals are calculated. The retrieval of the volume depolarization ratio is done by solving a system of two equations and two unknowns: the volume depolarization ratio at a reference height $\delta(z_0)$ and the volume depolarization ratio at all heights $\delta(z)$ (Reichardt et al., 2003).

In this extended 3-signal calibration procedure, the signals are not normalized to a reference height z_0, instead, we divide directly the signals, obtaining the ratios R_P, R_S and R_δ, by taking then the difference between two altitudes (and not the ratio) we subtract the crosstalk in the emission and reception (ε_l and ε_r) and the angular misalignment ($c_{2\alpha}$). The difference offers additionally a better performance in terms of error propagation compared to the ratio. In this way, the so called interchannel constants (X_δ, X_S and X_P) remain in the equations and they can be estimated by evaluating Eqs. (35), (36) and (37) respectively. Although we can estimate this three constants, we have to note that the number of unknowns are actually two X_P and X_S being the third constant X_δ the ratio of them (please see Eq. (30)), i.e. Eq.(35) is equivalent to Eq.(36) divided Eq. (37).

Given the form of Eqs. (35)-(37), observable differences between the height points z_j and z_k are needed for its evaluation, in practice, only altitude regions should be selected in the determination of X_P, X_S, and X_δ where significant changes in the depolarization ratio occur, e.g., in liquid-water clouds where multiple scattering by droplets produce steadily increasing depolarization with increasing penetration of laser light into the cloud (Donovan et al., 2015; Jimenez et al., 2017; Jimenez et al., 2018). Long measurements periods should be considered for the evaluation of Eqs. (35)-(37). All pair of data points (z_j and z_k in a certain height range, defined according to the ratio of signals) in all single measurements (in time t) provide an array with many observations of the interchannel constants, averaging these arrays we obtain a trustworthy estimate of these constants for the retrieval of the volume depolarization ratio (please see Figure 6).

To derive the linear depolarization ratio, we divide Eq. (25) by Eq. (24),

$$\frac{N_S}{N_P}\frac{\eta_{II,P}}{\eta_{\perp,S}} = X_\delta R_\delta = \frac{(1+\varepsilon_r)(1+\varepsilon_l)-\frac{(1-\delta)}{(1+\delta)}(1-\varepsilon_l)(1-\varepsilon_r)c_{2\alpha}}{(1+\varepsilon_r)(1+\varepsilon_l)+\frac{(1-\delta)}{(1+\delta)}(1-\varepsilon_l)(1-\varepsilon_r)c_{2\alpha}}. \quad (38)$$

Furthermore, we introduce the total crosstalk factor ξ_{tot},

$$\xi_{tot} = \frac{(1+\varepsilon_r)(1+\varepsilon_l)}{(1-\varepsilon_l)(1-\varepsilon_r)c_{2\alpha}} \geq 1, \quad (39)$$

which takes account for the combined effect of the emitted elliptically polarized wave front ε_l, of the angular misalignment between emitter and receiver (described by the rotation angle α), and of the crosstalk between receiver channels described by ε_r. The factor ξ_{tot} would be equal to 1 if the emitted laser pulses are totally linearly polarized, misalignment of the receiver unit could be avoided, and crosstalk between receiver channels are negligible.

Now Eq. (38) can be rewritten after dividing the numerator and denominator by $(1-\varepsilon_l)(1-\varepsilon_r)c_{2\alpha}$ and rearranging the equation:

$$X_\delta R_\delta = \frac{\xi_{tot}-\frac{(1-\delta)}{(1+\delta)}}{\xi_{tot}+\frac{(1-\delta)}{(1+\delta)}} \quad (40)$$

and the volume depolarization ratio can be obtained from Eq. (40) after rearrangement,

$$\delta(R_\delta, X_\delta, \xi_{tot}) = \frac{1-\xi_{tot}+X_\delta R_\delta(1+\xi_{tot})}{1+\xi_{tot}+X_\delta R_\delta(1-\xi_{tot})}. \quad (41)$$

As shown in Eq. (41), the volume depolarization ratio can be calculated by using the ratio R_δ between the cross and co-polarized signals and when the constants X_δ and ξ_{tot} are known. As first step of the calibration, the inter-channel constant X_δ (together with X_P and X_S) is obtained from the measurements by evaluating Eqs. (35)-(37) in the selected height range (with variations on the depolarization) at each measurement time t. Then ξ_{tot} can be estimated in a region (defined by height z_{mol}) with dominating Rayleigh backscattering for which the volume depolarization ratio, δ_{mol}, is assumed as constant and known. Behrendt et al. (2002) estimated theoretically a value of the linear depolarization ratio caused by molecules of 0.0046 for a lidar system whose interference filters have a FWHM=1.0 nm, however, Freudenthaler et al. (2016b) has found a value of 0.005 ± 0.012 based on long-term measurements in aerosol and cloud-free tropospheric height regions. We used this value and we have considered the propagation of this systematic uncertainty in our calculations. From, Eq. (41) ξ_{tot} is given by.

$$\xi_{tot} = \left(\frac{1-\delta_{mol}}{1+\delta_{mol}}\right)\left(\frac{1+X_\delta R_\delta(z_{mol})}{1-X_\delta R_\delta(z_{mol})}\right), \quad (42)$$

By calculating the ratio between Eqs. (24) and (26) (co to total) or the ratio between Eqs. (25) and (26) (cross to total), the volume depolarization ratio can also be derived:

$$\delta(R_S, X_S, \xi_{tot}) = \frac{1-\xi_{tot}(1-2X_S R_S)}{1+\xi_{tot}(1-2X_S R_S)}, \quad (43)$$

$$\delta(R_P, X_P, \xi_{tot}) = \frac{1-\xi_{tot}(2X_P R_P-1)}{1+\xi_{tot}(2X_P R_S-1)}. \quad (44)$$

In summary, the volume linear depolarization ratio can be calculated after the determination of the constants X_P, X_S, X_δ and

ξ_{tot}. Then the signal ratio profiles $R_P(z)$, $R_S(z)$, and $R_\delta(z)$ are required and calculated within Eqs. (31), (32) and (33), and by considering Eqs. (41), (43) and (44) the depolarization ratio can be finally calculated by using either the pair of signals N_S and N_P, the pair N_S and N_{tot}, or the pair N_P and N_{tot} respectively. However, the expected errors in the retrievals are not the same for all this pairs, since they present different sensitivities to changes in the depolarization ratio, obtaining the largest uncertainties when the pair N_P and N_{tot} is used.

4 Observations

4.1 Application of the calibration approach to a measurement case

To test the method introduced in Sect. 3, the measurement case from 19 September 2017 was analyzed and the results are presented in this section. Figure 4 provides an overview of the atmospheric situation. An aerosol layer reached up to about 2.8 km height and was topped by a persistent, shallow altocumulus deck with cloud base height at 2.6-2.7 km a.g.l. (above ground level)

Although the time resolution of the lidar measurements is 30 seconds, to reduce computing time and signal noise, we consider 5 minutes average measurements. Figure 5 shows as example the three range-corrected signals of the polarization lidar, the signal ratios as defined by Eqs. (31)-(33), and the corresponding inverse ratios for a 5-minute measurement.

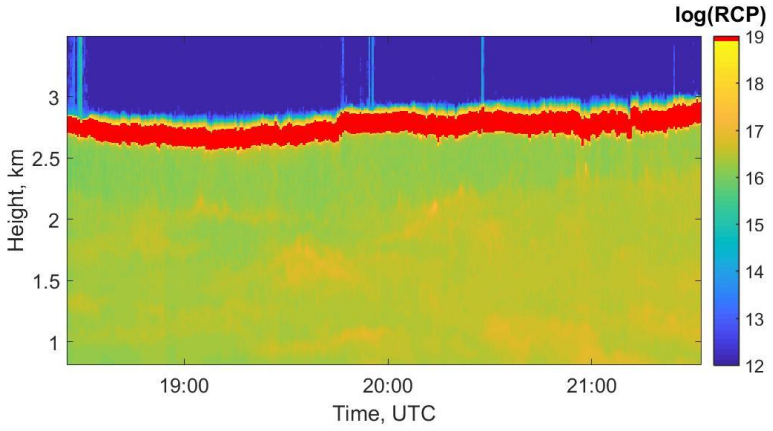

Figure 4: Range-corrected 532 nm total backscatter signal (RCP) measured on 19 September 2017 with 30 s and 7.5 m vertical resolution.

In the next step of the data analysis and calibration procedure, we selected the height range from a few meters below cloud base up to 240 meters above cloud base for each 5-minute averaging period *t*, then we computed the instrumental inter-channel ratios $X_P(z_j, z_k, t)$, $X_S(z_j, z_k, t)$, and $X_\delta(z_j, z_k, t)$ with Eqs. (37), (36), and (35), respectively. Height resolution was 7.5 m. The result is shown in Fig. 6.

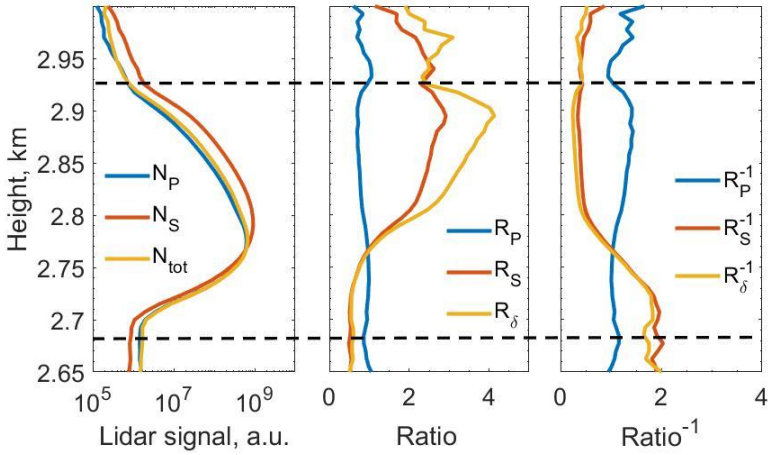

Figure 5: Example of a 5-minute profile of range-corrected lidar signals from the channels, signal ratios, and inverse ratios. The calibration procedure considers all signals of the 3-hour measurement period shown in Fig. 4. The dash line indicates the range where the calibration calculations where done.

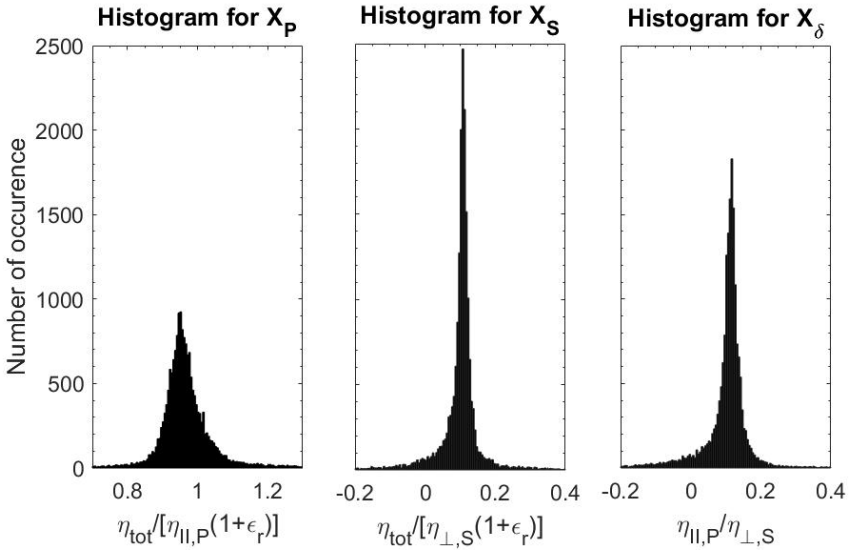

Figure 6: Histograms for the inter-channel constants X_P, X_S and X_δ. Each point corresponds to a combination z_j and z_k in a 5-minute period, obtaining about 18000 data points for this 3-hour measurement case.

The mean values of the constants with the respective statistical error based on Fig. 6 are: $X_P = 0.965 \pm 0.012$, $X_S = 0.108 \pm 0.005$ and $X_\delta = 0.110 \pm 0.006$. The reason for these low uncertainties is that the calibration is performed in a cloudy region so that every channel shows high count rates and thus high signal-to-noise ratios.

Using the constant X_δ and evaluating Eq. (42) in the particle-free region of the 3-hour measurement period, a mean value of $\xi_{tot} = 1.118 \pm 0.008$ for the total crosstalk was obtained. Given the form of the equations to retrieve the profiles of volume depolarization ratio (Eqs. (35)-(37)), the propagated uncertainty associated to ξ_{tot} does not vary largely with height, which leads to a large percentage uncertainty on the retrieval of the volume linear depolarization ratio in the region with low depolarization ratios, also characterized by low signal strengths. Table 1 summarize the retrieved instrumental constants for the measurement case presented.

Table 1: Values of the instrumental inter-channel constants and crosstalk factor determined for the measurement case presented.

Instrumental constant	Value
$\boldsymbol{X_P}$	0.965 ± 0.012
$\boldsymbol{X_S}$	0.108 ± 0.005
$\boldsymbol{X_\delta}$	0.110 ± 0.006
$\mathfrak{E}_{tot}$	1.118 ± 0.008

Figure 7 presents the height profiles of the volume linear polarization ratio computed by means of Eqs. (41), (43), and (44). Good agreement between the different solutions is visible. However, the depolarization ratios obtained from the channels N_p and N_{tot} (blue) shows the largest uncertainties, especially above the cloud layer. The profile-mean absolute uncertainties from the ground up to the cloud top (3.1 km) for $\delta(R_P, X_P)$, $\delta(R_S, X_S)$ and $\delta(R_\delta, C)$ are 0.034, 0.0139 and 0.0137, respectively. The three derived depolarization ratios agree well in the cloud region, differences appear in the upper part of the cloud caused by strongly reduced count rates due to the strong attenuation of all the channels, in order to avoid signal saturation at low level clouds.

Figure 8 presents the volume depolarization ratio with 30 s temporal resolution. The signal ratio R_δ and the constant X_δ where used. These profiles are the basis for the retrieval of the microphysical properties of the liquid-water cloud. The results will be discussed in a follow-up article (Jimenez et al., 2018b).

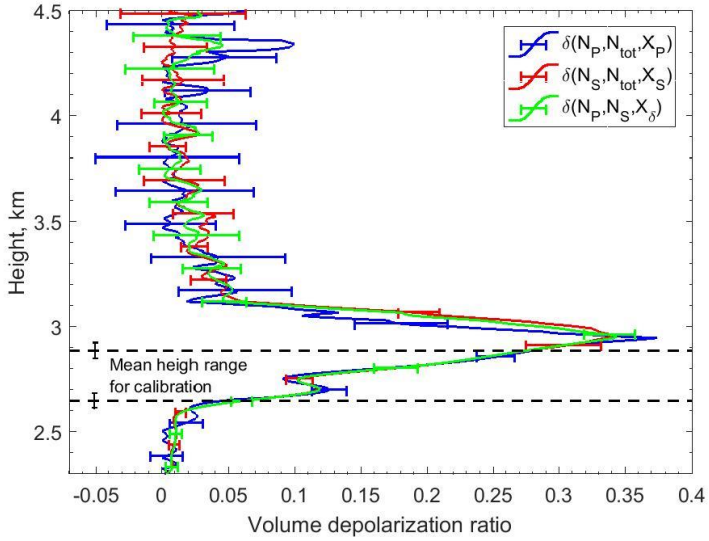

Figure 7: Profiles of the volume linear depolarization ratio for the 3 hours period in the cloud region, using the three pairs of signal ratios presented in Eqs. (41), (43) and (44). The error bars include the statistical and systematical uncertainties. The dash lines indicate the mean height range (of 240 meters) where the calculation of the interchannel constants was performed.

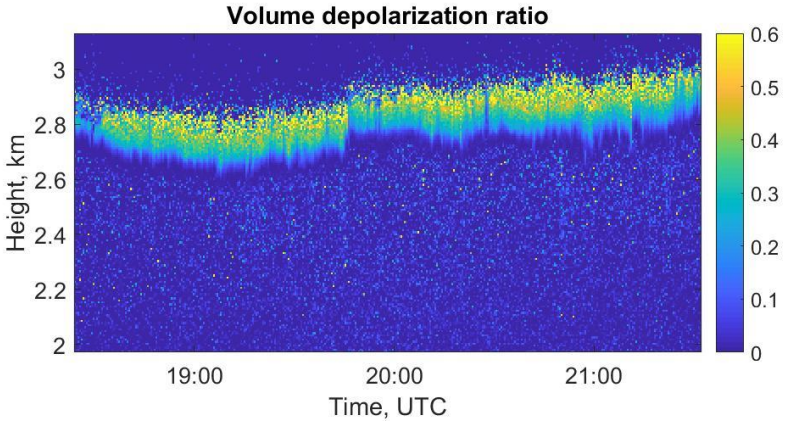

Figure 8: Volume linear depolarization ratio for the entire 3-hour period, shown in Fig. 4. The temporal resolution is 30 seconds.

To validate the new system and the calibration procedure a comparison between the measurements of the volume linear depolarization ratio with the lidar systems MARTHA and BERTHA (Backscatter Extinction Lidar Ratio Temperature and Humidity profiling Apparatus) is presented in Figure 9. The observations were conducted at Leipzig (51°N, 12°E) on 29 May 2017 with the presence of a Dust layer between 2 and 5 km and a cirrus cloud at 11 km (see Fig. 9a). Good agreement in the dust layer can be noted, while the cirrus cloud shows differences between the two systems, that difference can be attributed to the fact that the BERTHA system is pointing 5° respect to the zenith, while the MARTHA system points to the Zenith (0°).

This could lead to specular reflection by horizontally oriented ice crystals reducing the depolarization ratio in the case of the MARTHA system.

A second measurement period during an unique event with a dense biomass burning smoke layer in the stratosphere on 22 August 2017 was considered for comparison (Haarig et al., 2018), here very good agreement for the layer between 5 and 7 km and also for the layer at 14 km was obtained, confirming the good performance of the systems and of the respective calibration procedures, extended 3-signal method in MARTHA and the Δ90° method in the BERTHA system.

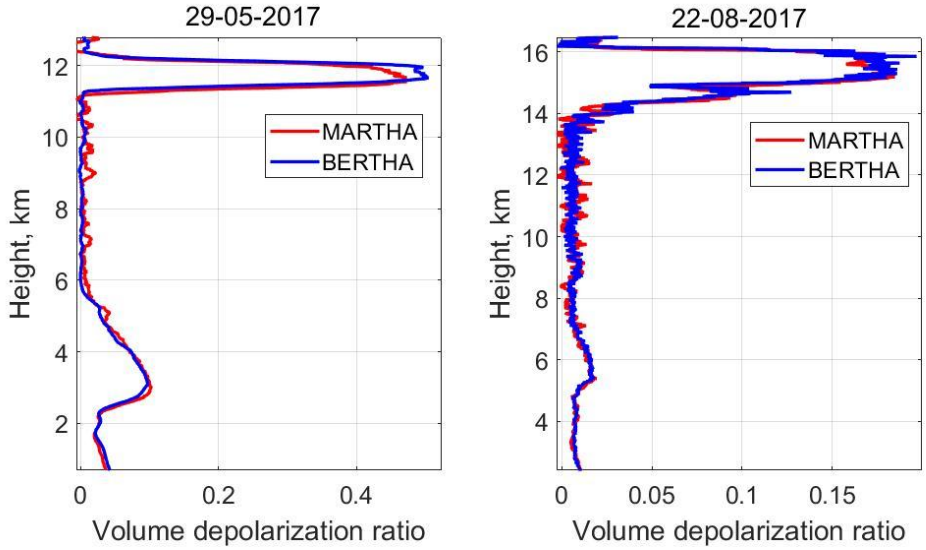

Figure 9: Volume linear depolarization ratio obtained with MARTHA (extended 3-signal method) and BERTHA (Δ90° method) on (a) 29 May 2017 20:20-20:45 (with smooth 27 bins) (b) 22 August 2017 20:45-23:15 (Haarig et al., 2018). The systems were calibrated independently. The system were located at a distance of 80 meters.

4.2 Temporal stability of the polarization lidar calibration and performance

The time series of the inter-channel constant X_δ obtained from MARTHA observations between day 120 and 320 of 2017 is presented in Fig. 10. The respective time series of ξ_{tot} is given in Fig. 11. As can be seen, the calibrations values show the lowest uncertainties in the inter-channel constants (of about 4%) when altocumulus layers with a stable cloud base and moderate light extinction were present. Higher uncertainty levels were observed in the case of cirrus clouds (green, 11%) and the Saharan dust layer. In the case of very thick cumulus clouds (black), the mean uncertainty was 21%. One reason for these differences in the uncertainty of X_δ is that the system was optimized for the observation of low-altitude liquid-water clouds, for which the detection channels need large attenuation to avoid saturation of the detectors in the cloud layer. This setup prohibited an optimum detection of high-level dust layers and ice clouds due to the low signal strength for these cases. Furthermore, liquid clouds are favorable for calibration because the volume depolarization ratio increases very smoothly as a

result of the increasing multiple scattering impact. At these conditions, a large number of measurement pairs for heights z_j and z_k with different depolarization ratios are available. Some slight changes of X_δ occurred when the attenuation configuration of the polarization receivers was changed. Small day-to-day changes were caused by small variations in the response of each detector with time.

In Fig. 10 are the retrieved values of ξ_{tot}, small variations can be seen but they remain much lower than the uncertainties, and no stronger variations can be noted with changes in the attenuation or changes of the calibration medium (water cloud, cirrus, Saharan dust layer). In 2017, the mean value $\xi_{tot} = 1.109 \pm 0.009$.

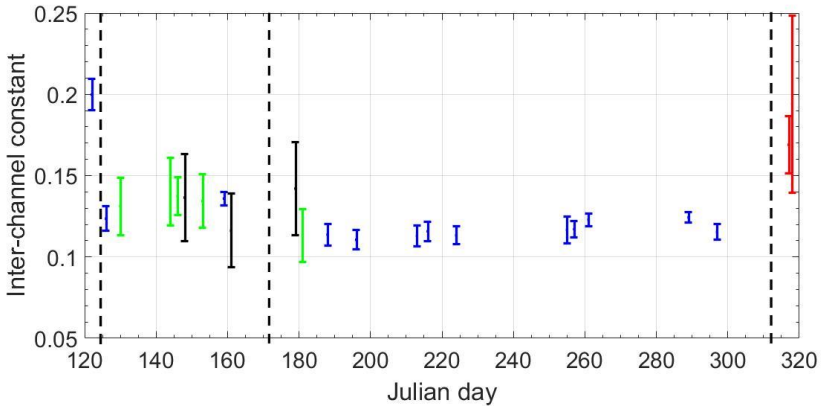

Figure 10: Time series of the inter-channel calibration constant X_δ measured from end of April to mid November 2017. The vertical bars show the uncertainty in the retrieval. The calibration procedure was based on lidar measurements in liquid-water clouds (blue), cirrus clouds (green), during optically thick cumulus events (black), and Saharan dust periods (red). The dash lines indicate the days where changes in the attenuation configuration of the channels were made.

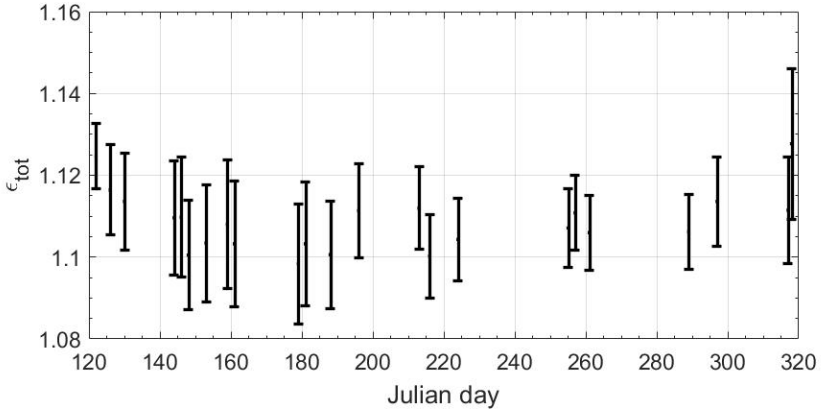

Figure 11: Time series of the total crosstalk factor ε_{tot} measured in 2017. The vertical bars show the uncertainty in the retrieval, which include the statistical error from the determination of the inter-channel constants and systematical errors from the value considered in the molecular region 0.005 ± 0.0012.

5 Summary and conclusions

In this work a new formalism to calibrate polarization lidar systems based on three detection channels has been presented. We propose a simple lidar polarization receiver, based on three telescopes (one for each channel) with a polarization filter on the front (in the case of the cross and co polarized channels), this set up removes the effect of the receiver optics on the polarization state of the collected backscattered light, simplifying the measurement concept. The derivation of the volume linear depolarization ratio considering the instrumental effects on the proposed system was described in Sect. 3, here there are three effects considered: the emitted laser beam (after beam expander) is slightly elliptically polarized ($\mathcal{E}_l$), there is an angular misalignment (α) of the receiver unit with respect to the main polarization plane of the emitted laser pulses and there is a small crosstalk amount in the detection channels (co and cross) ($\mathcal{E}_r$). These instrumental parameters can be summarized into one single constant, the so-called total crosstalk (ξ_{tot}).

The methodology does not require a priori knowledge about the behavior of the instrument in terms of polarization and permits the determination of the so-called inter-channel constants X_P, X_S and X_δ, which depend on the attenuation and detector response of each channel, and thus it is expected to vary between different measurement days. In the free-aerosol region the total crosstalk can also be estimated by means of long term measurements, in our case we estimated a mean value of $\xi_{tot} = 1.109 \pm 0.009$. The calibration is based on actual lidar measurement periods, providing large amount of input data for accurate estimation of the mean value of the instrumental constants. However, it needs a strong depolarizing medium for its application, such as dust layers and also water clouds, which depolarize the light due to multiple scattering in droplets or due to single scattering of ice particles.

A case study of a liquid-water cloud observation was presented, the 3-hours period demonstrates the potential of the new technique for the retrieval of accurate high temporal resolution depolarization profiles. The method is simple to implement and allows high quality depolarization ratio studies. Temporal studies indicated the robustness and stability of the three-signal lidar system over long time periods. A comparison with a second polarization lidar shows excellent agreement regarding the derived volume linear polarization ratio of biomass burning smoke throughout the troposphere and the lower stratosphere up to 16 km height.

Appendix A: General case regarding the rotation of the polarization filters with respect to the true polarization axis of the emitted light

For the derivation outlined in Sect. 3 it is assumed that the polarization filters in front of the cross- and co-polarized telescopes are pointing 90° with respect to each other. However, in the general case, when their angular deviation with respect to their respective components is different (E_P to E_{II} and E_S to $E_\perp$), Eqs. (24) and (25) have a different angular component. In this appendix we analyze this general case and discuss the need of implementation depending on the results obtained.

We define the angles α_P and α_S as the angular misalignment of the channels E_P and E_S with respect to E_{II} and $E_\perp$ respectively (see Fig A1). We rewrite Eqs. (24) - (26), we factorize by $(1+\varepsilon_r)$ and to simplify the expression, we adopt the polarization parameter $a = \frac{(1-\delta)}{(1+\delta)}$ again. We do not use the short notation of the cosine adopted in Sect.3.

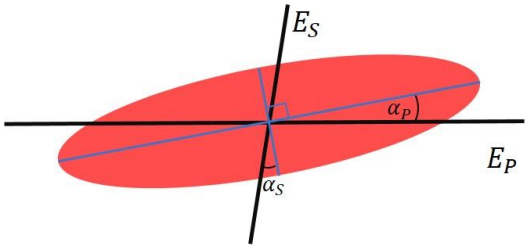

Figure A1: Scheme of the observation of the polarization state of the backscattered light (similar to Fig. 3), the co and cross channels are misaligned with respect to their components in an angle α_P and α_S respectively.

$$\frac{N_P(z)z^2}{\eta_{II,P}\,P_0T^2(z)} = \beta_{II,in}(z) + \varepsilon_r\beta_{\perp,in}\,(z) = (1+\varepsilon_r)\left(1 + a(z)\,\frac{(1-\varepsilon_l)}{(1+\varepsilon_l)}\frac{(1-\varepsilon_r)}{(1+\varepsilon_r)}\cos(2\alpha_P)\right)\beta(z)/2, \quad \text{(A1)}$$

$$\frac{N_\perp(z)z^2}{\eta_{\perp,S}P_0T^2(z)} = \beta_{\perp,in}(z) + \varepsilon_r\,\beta_{II,in}(z) = (1+\varepsilon_r)\left(1 - a(z)\frac{(1-\varepsilon_l)}{(1+\varepsilon_l)}\frac{(1-\varepsilon_r)}{(1+\varepsilon_r)}\cos(2\alpha_S)\right)\beta(z)/2, \quad \text{(A2)}$$

$$\frac{N_{tot}(z)z^2}{\eta_{tot}P_0T^2(z)} = \beta_{in}(z) = \beta(z). \quad \text{(A3)}$$

In a similar way as we defined ξ_{tot}, we define the total crosstalk factor for the co and cross polarized channels respectively.

$$\xi_P = \frac{(1+\varepsilon_r)(1+\varepsilon_l)}{(1-\varepsilon_l)(1-\varepsilon_r)\cos(2\alpha_P)} \geq 1, \quad \text{(A4)}$$

$$\xi_S = \frac{(1+\varepsilon_r)(1+\varepsilon_l)}{(1-\varepsilon_l)(1-\varepsilon_r)\cos(2\alpha_S)} \geq 1, \quad \text{(A5)}$$

The three-signal polarization equation (Eq. (27)) can be rewritten in a general form, when adding Eqs. (A1) and (A2) and considering Eq. (A3):

$$\left(\frac{N_P(z)}{\eta_{II,P}} + \frac{N_S(z)}{\eta_{\perp,S}}\right) = (1+\varepsilon_r)(1 + a(z)(\xi_P^{-1} - \xi_S^{-1})/2)\,\frac{N_{tot}(z)}{\eta_{tot}}. \quad \text{(A6)}$$

The term $\xi_P^{-1} - \xi_S^{-1}$ depends on the difference of the cosines of $2\alpha_P$ and $2\alpha_S$, we define the parameter ξ_S^P which account for the difference of the impact of the polarization channels.

$$\xi_S^P \coloneqq (\xi_P^{-1} - \xi_S^{-1})/2 = \frac{(1-\varepsilon_l)(1-\varepsilon_r)}{2(1+\varepsilon_l)(1+\varepsilon_r)}(\cos(2\alpha_P) - \cos(2\alpha_S)). \quad \text{(A7)}$$

This factor can be positive or negative, depending on which polarization filter is more misaligned, and it is equal to zero when they point 90° with respect to each other. Eq. (A6) can be expressed as:

$$\left(\frac{N_P(z)}{\eta_{II,P}} + \frac{N_S(z)}{\eta_{\perp,S}}\right) = (1+\varepsilon_r)(1 + \xi_S^P a(z))\,\frac{N_{tot}(z)}{\eta_{tot}}, \quad \text{(A8)}$$

We adopt the notation:

$$\Delta R_P(z_j, z_k) = R_P(z_j) - R_P(z_k), \quad \text{(A9)}$$

for account the difference between the signal ratios R_P, R_S and R_δ, between the polarization parameter a, and between the ratios a/R_S and a/R_P at the heights z_j and z_k. In an equivalent way as we derived Eqs. (35)-(37) we can obtain a general solution for the instrumental inter-channel constants:

$$X_P(z_j, z_k) = \frac{\Delta R_S^{-1}(z_k) + \xi_S^P \, \Delta\left(\frac{a}{R_S}(z_j, z_k)\right)}{\Delta R_\delta^{-1}(z_j, z_k)}, \tag{A10}$$

$$X_S(z_j, z_k) = \frac{\Delta R_P^{-1}(z_j, z_k) + \xi_S^P \, \Delta\left(\frac{a}{R_P}(z_j, z_k)\right)}{\Delta R_\delta\,(z_j, z_k)}, \tag{A11}$$

$$X_\delta(z_j, z_k) = \frac{\Delta R_P\,(z_j, z_k) + \xi_S^P \frac{\Delta a(z_j, z_k)}{2X_P}}{\Delta R_S^{-1}(z_j, z_k)}, \tag{A12}$$

In an absolute sense it would not be possible to determine the inter-channel constants X_P, X_S and X_δ without knowing the polarization parameter (or the depolarization ratio), however, the impact on Eqs. (A10) - (A12) of their respective second term can be very small, since it depends on the difference of the cosines of small angles. For example, if $2\alpha_P = 5°$ and $2\alpha_S = 10°$, using Eq. (A7) $\xi_S^P = 0.005 \frac{(1-\varepsilon_l)(1-\varepsilon_r)}{(1+\varepsilon_l)(1+\varepsilon_r)}$. Considering this small effect, a first guess of the polarization parameter would be sufficient to solve equations (A10) - (A12).

Calculating the three ratios between Eqs. (A1), (A2) and (A3), we can obtain the volume linear depolarization ratio, similarly as how it was done for Eqs. (41), (43) and (44).

$$\delta(R_S, X_S, \xi_S) = \frac{1-\xi_S(1-2X_S R_S)}{1+\xi_S(1-2X_S R_S)}, \tag{A13}$$

$$\delta(R_P, X_P, \xi_P) = \frac{1-\xi_P(2X_P R_P - 1)}{1+\xi_P(2X_P R_P - 1)}, \tag{A14}$$

$$\delta(R_\delta, X_\delta, \xi_P, \xi_S) = \frac{1+\frac{\xi_S}{\xi_P} X_\delta R_\delta \; - \xi_S(1-X_\delta R_\delta)}{1+\frac{\xi_S}{\xi_P} X_\delta R_\delta + \xi_S(1-X_\delta R_\delta)}. \tag{A15}$$

$$a = \frac{1-\delta}{1+\delta}, \tag{A16}$$

In the measurement example presented, we performed an iterative computation procedure to determine the inter-channel calibration constants and the crosstalk factors. Using Eqs. (A10)-(A12), in a first run we determined the inter-channel constants when we assume ξ_S^P=0, i.e. $\theta_P = \theta_S$, a first guess of the volume depolarization ratio using each pair of signals is obtained (Eqs. (A13)- (A15)), then the corresponding crosstalks ξ_P and ξ_S are determined by imposing a mean value of $\delta = 0.005 \pm 0.012$ in the free aerosol region (Freudenthaler et al., 2016b). The second run takes the values of $\xi_S^P \neq 0$ and of the polarization parameter $a(z,t)$ (Eqs. (A14) and (A16)) from the first run and the inter-channel constants are computed again. Figure A2 shows the results of performing the calibration iteratively. Small differences between the values obtained in the first and second run can be noted, in fact, the variations are smaller than the error of the respective constants, and we can see that after the second run, all values remain practically constant. The mean values of the instrumental constants after 6 iterations are listed in the Table A1.

In this measurement case we found a value for $\xi_S^P = -0.008$. Due to this small value there are no important variations between the first guess and the second run, therefore we conclude that by assuming $\xi_S^P = 0$ a fast and practical inversion procedure is possible. However, in cases with larger differences between α_P and α_S, an iterative procedure as described above would be needed.

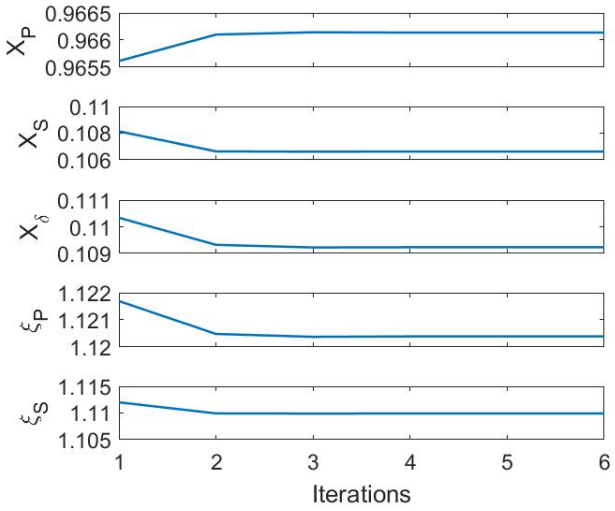

Figure A2: Instrumental channels obtained with an iterative procedure. We did not include the error bars since they are much larger than the variations between runs.

This general solution for the lidar three-signal problem converge to the same results when we also consider that the receiver crosstalk can be eventually different for the channels P and S. In that case we would have $\varepsilon_{r,P}$ and $\varepsilon_{r,S}$ which would also lead to two constants ξ_P and ξ_S to determine. For simplicity we talked in this section only about the effect of the different angular misalignment of the channel.

Table A1: Results of the instrumental constants after using the iterative procedure (6 runs)

Instrumental constant	Value
$\boldsymbol{X_P}$	0.966 ± 0.011
$\boldsymbol{X_S}$	0.106 ± 0.005
$\boldsymbol{X_\delta}$	0.109 ± 0.006
$\boldsymbol{\xi_P}$	1.120 ± 0.007
$\boldsymbol{\xi_S}$	1.110 ± 0.007

Appendix B

Table B1: Description of the variables used in the approach.

Variable	Description
$\boldsymbol{z}$	Height.
$\boldsymbol{a}$	Atmospheric polarization parameter. Varies with height z.
$\boldsymbol{\delta}$	Atmospheric volume depolarization ratio, so that $\delta = \frac{1-a}{1+a}$.
$\boldsymbol{\delta_{mol}}$	Volume depolarization ratio in the free-aerosol region. Assumed constant and known.
$\boldsymbol{\beta}$	Backscattering coefficient. Equal to the element F_{11} from the atmospheric scattering matrix.
$\boldsymbol{\beta_{in}}$	Backscatter that arrives the receiver and it is measured by the total channel, $\beta_{in} = \beta$ in our system ($D_{tot} = 1$)
$\boldsymbol{\beta_{II,in}}$	Parallel component of the arriving backscatter (with respect to the axis P).
$\boldsymbol{\beta_{\perp,in}}$	Cross component of the arriving backscatter (with respect to the axis S).
T	Atmospheric transmission path for the lidar equation.
$\boldsymbol{P_0}$	Number of emitted photons.
$\boldsymbol{\varepsilon_l}$	Portion of the emitted radiation polarized in the cross direction ($\perp$), called crosstalk of the emitter.
$\boldsymbol{I_L}$	Stokes vector describing the emitted radiation in term of the polarization state.
F	Scattering matrix of the atmosphere. The element F_{11} corresponds to the backscattering coefficient β.
$\boldsymbol{I_{in}}$	Stokes vector describing the arriving radiation after being transmitted, backscattered and depolarized by the atmosphere.
$\boldsymbol{c_{2\alpha}}$	$\cos(2\alpha)$, α denotes the rotation between the polarization axis of the emission respect to the reception.
$\mathbf{R}(\boldsymbol{\alpha})$	Rotation matrix to consider the effect of the rotation α between emission and receiver polarization plane.
$\boldsymbol{N_i(z)}$	Number of photons measured by each detector (i=P, S, tot) at height z.
$\boldsymbol{\eta_{II,P}}$	Constant describing the efficiency of the channel P to the component II.
$\boldsymbol{\eta_{\perp,S}}$	Constant describing the efficiency of the channel S to the component $\perp$.
$\boldsymbol{\eta_{tot}}$	Constant describing the efficiency of the total channel (tot) to the sum of the components $II+\perp$.
$\boldsymbol{D_i}$	Efficiency ratio of each channel, $= \boldsymbol{\eta_{\perp,i}/\,\eta_{II,i}}$ **(i = P,S).** $D_{tot} \equiv 1$ (ideal).
$\boldsymbol{\varepsilon_r}$	So called crosstalk of the receiver. $\varepsilon_r = D_P = D_S^{-1}$ (ideal case).
$\boldsymbol{X_P}$	So-called interchannel constant, similar to the gain ratio used in previous studies (η^*). $\eta_{tot}/[\eta_{II,P}(1+\varepsilon_r)]$

$\boldsymbol{X_S}$	$\eta_{tot}/[\eta_{\perp,S}(1+\varepsilon_r)]$
$\boldsymbol{X_\delta}$	$\eta_{II,P}/\eta_{\perp,S} = X_S/X_P$
$\boldsymbol{R_P}$	Ratio of signals $N_P(z)/N_{tot}(z)$
$\boldsymbol{R_S}$	Ratio of signals $N_S(z)/N_{tot}(z)$
$\boldsymbol{R_\delta}$	Ratio of signals $N_S(z)/N_P(z)$
$\boldsymbol{\xi_{tot}}$	So called total crosstalk of the system (ideal case). It summarizes the 3 instrumental effects considered ($\varepsilon_l, c_{2\alpha}$ and ε_r).
$\boldsymbol{\xi_P}$	Total crosstalk of the P channel (non-ideal case).
$\boldsymbol{\xi_S}$	Total crosstalk of the S channels (non-ideal case).
$\boldsymbol{\xi_S^P}$	$= (\xi_P^{-1} - \xi_S^{-1})/2$
$\boldsymbol{\Delta R_i(z_j, z_k)}$	$= R_P(z_j) - R_S(z_k)$

Additional information about the extended 3-signal calibration approach.

- The extinction coefficient is assumed to be independent of the polarization state of the light. This assumption permits the simplification of the three lidar equations making possible the determination of the instrumental constants.
- The effects of the emission and reception in terms of polarization can be summarized into one total crosstalk constant ξ_{tot} (in the ideal case), or into two total crosstalk ξ_P and ξ_S for the non-ideal case (Appendix A).
- Differences with previous studies in terms of the nomenclature are present:
  - In our approach ε to denotes crosstalk, and not the error angle of the $\Delta 90$ calibration as denoted in previous studies. The crosstalk has been usually denoted by G_S and H_S (Freudentaler, 2016).
  - D_i denotes the efficiency ratio (Reichardt et al., 2003), while in recent studies D denotes the diattenuation parameter.
- The total channel is assumed to be ideal in terms of polarization, i.e. $D_{tot} = 1$.
- No diattenuation and retardation is considered in the emission and reception units.

References

Behrendt, A., and Nakamura, T.: Calculation of the calibration constant of polarization lidar and its dependency on atmospheric temperature, Opt. Express, 10, 805-817, 2002.

Belegante, L., Bravo-Aranda, J. A., Freudenthaler, V., Nicolae, D., Nemuc, A., Ene, D., Alados-Arboledas, L., Amodeo, A., Pappalardo, G., D'Amico, G., Amato, F., Engelmann, R., Baars, H., Wandinger, U., Papayannis, A., Kokkalis, P., and

Pereira, S. N.: Experimental techniques for the calibration of lidar depolarization channels in EARLINET, Atmos. Meas. Tech., 11, 1119-1141, https://doi.org/10.5194/amt-11-1119-2018, 2018.

Biele, J., Beyerle, G., and Baumgarten, G.: Polarization lidar: Corrections of instrumental effects, Opt. Express, 7,427-435, 2000.

Bissonnette, L. R., Bruscaglioni, P., Ismaelli, A., Zaccanti, G., Cohen, A., Benayahu, Y., Kleiman, M., Egert, S., Flesia, C., Schwendimann, P., Starkov, A. V., Noormohammadian, M., Oppel, U. G., Winker, D. M., Zege, E. P., Katsev, I. L., and Polonsky, I. N.: LIDAR multiple scattering from clouds, Appl. Phys. B, 60, 355-362, https://doi.org/10.1007/BF01082271, 1994.

Bravo-Aranda, J. A., Belegante, L., Freudenthaler, V., Alados-Arboledas, L., Nicolae, D., Granados-Muñoz, M. J., Guerrero-Rascado, J. L., Amodeo, A., D'Amico, G., Engelmann, R., Pappalardo, G., Kokkalis, P., Mamouri, R., Papayannis, A., Navas-Guzmán, F., Olmo, F. J., Wandinger, U., Amato, F., and Haeffelin, M.: Assessment of lidar depolarization uncertainty by means of a polarimetric lidar simulator, Atmos. Meas. Tech., 9, 4935-4953, https://doi.org/10.5194/amt-9-4935-2016, 2016.

Chen, W. N., Chiang, C. W., Nee, J. B.: Lidar ratio and depolarization ratio for cirrus clouds, Appl. Opt., 41, 6470-6476, https://doi.org/10.1364/AO.41.006470, 2002.

Chipman, R. A.: Mueller matrices in: Handbook of Optics, Volume I, 3rd Edn., chap. 14, McGraw-Hill, 2009.

David, G., Miffre, A., Thomas, B., and Rairoux, P.: Sensitive and accurate dual-wavelength UV-VIS polarization detector for optical remote sensing of tropospheric aerosols, Appl. Phys. B, 108, 197–216, https://doi.org/10.1007/s00340-012-5066-x, 2012.

Donovan, D. P., Klein Baltink, H., Henzing, J. S., de Roode, S. R., and Siebesma, A. P.: A depolarisation lidar-based method for the determination of liquid-cloud microphysical properties, Atmos. Meas. Tech., 8, 237-266, https://doi.org/10.5194/amt-8-237-2015, 2015.

Eloranta, E. W.: Practical model for the calculations of multiply scattered lidar returns, Appl. Optics, 37, 2464-2472, 1998.

Engelmann, R., Kanitz, T., Baars, H., Heese, B., Althausen, D., Skupin, A., Wandinger, U., Komppula, M., Stachlewska, I. S., Amiridis, V., Marinou, E., Mattis, I., Linné, H., and Ansmann, A.: The automated multiwavelength Raman polarization and water-vapor lidar PollyXT: the neXT generation, Atmos. Meas. Tech., 9, 1767–1784, https://doi.org/10.5194/amt-9-1767-2016, 2016.

Fan J., Wang Y., Rosenfeld D., and Liu X.: Review of Aerosol-Cloud Interactions: Mechanisms, significance, and Challenges, J. Atmospheric Sci., 73, 4221-4252, https://doi.org/10.1175/JAS-D-16-0037.1, 2016.

Freudenthaler, V., Esselborn, M., Wiegner, M., Heese, B., Tesche, M., Ansmann, A., Müller, D., Althausen, D., Wirth, M., Fix, A., Ehret, G., Knippertz, P., Toledano, C., Gasteiger, J., Garhammer, M., and Seefeldner, M.: Depolarization ratio profiling at several wavelengths in pure Saharan dust during SAMUM 2006, Tellus B, 61, 165–179, https://doi.org/10.1111/j.1600- 0889.2008.00396.x, 2009.

Freudenthaler, V.: About the effects of polarising optics on lidar signals and the Δ90 calibration, Atmos. Meas. Tech., 9, 4181-4255, https://doi.org/10.5194/amt-9-4181-2016, 2016.

Freudenthaler, V., Seefeldner, M., Groß, S., and Wandinger., U.: Accuracy of Linear Depolarisation Ratios in Clean Air Ranges Measured with POLIS-6 at 355 and 532 NM, EPJ Web of Conferences 119, 25013, https://doi.org/10.1051/epjconf/201611925013, 2016b.

Groß, S., Freudenthaler, V., Schepanski, K., Toledano, C., Schäfler, A., Ansmann, A., and Weinzierl, B.: Optical properties of long-range transported Saharan dust over Barbados as measured by dual-wavelength depolarization Raman lidar measurements, Atmos. Chem. Phys., 15, 11067-11080, https://doi.org/10.5194/acp-15-11067-2015, 2015.

Haarig, M., Ansmann, A., Althausen, D., Klepel, A., Groß, S., Freudenthaler, V., Toledano, C., Mamouri, R.-E., Farrell, D. A., Prescod, D. A., Marinou, E., Burton, S. P., Gasteiger, J., Engelmann, R., and Baars, H.: Triple-wavelength depolarization-ratio profiling of Saharan dust over Barbados during SALTRACE in 2013 and 2014, Atmos. Chem. Phys., 17, 10767-10794, https://doi.org/10.5194/acp-17-10767-2017, 2017.

Haarig, M., Ansmann, A., Baars, H., Jimenez, C., Veselovskii, I., Engelmann, R., and Althausen, D.: Depolarization and lidar ratios at 355, 532, and 1064 nm and microphysical properties of aged tropospheric and stratospheric Canadian wildfire smoke, Atmos. Chem. Phys., 18, 11847-11861, https://doi.org/10.5194/acp-18-11847-2018, 2018.

Hogan, R. J.: Fast Lidar and Radar Multiple-Scattering Models. Part I: Small-Angle Scattering Using the Photon Variance-Covariance Method, J. Atm. Sci., 65, 3621-3635, 2008.

Hogan, R. J., Haywood, J. M., Westbrook, C. D., Dacre, H. F., Marenco, F., O'Connor, E. J., Johnson, B. T., Wrench, C. L., and Belcher, S. E.: Combined lidar and sun photometer retrievals of ash particle size and mass concentration from the Eyjafjallajökull volcano, J. Geophys. Res., in press, 2012.

Hu, Y., Vaughan, M., Liu, Z., Lin, B., Yang, P., Flittner, D., Hunt, B., Kuehn, R., Huang, J., Wu, D., Rodier, S., Powell, K., Trepte, C., and Winker, D.: The depolarization – attenuated backscatter relation: CALIPSO lidar measurements vs. theory, Opt. Express 15, 5327–5332, 2007.

Huang, Y., Chameides, W. L., and Dickinson, R. E.: Direct and indirect effects of anthropogenic aerosols on regional precipitation over east Asia, J. Geophys. Res., 112, D03212, doi:10.1029/2006JD007114, 2007.

IPCC: Climate Change 2014: Synthesis Report. Contribution of Working Groups I, II and III to the Fifth Assessment Report of the Intergovernmental Panel on Climate Change, edited by: Core Writing Team, Pachauri, R.K., and Meyer, L.A., IPCC, Geneva, Switzerland, 151 pp; available at: https://www.ipcc.ch/pdf/assessment-report/ar5/syr/SYR_AR5_FINAL_full.pdf, 2014.

Jimenez, C., Ansmann, A., Donovan, D., Engelmann, R., Malinka, A., Schmidt, J., and Wandinger, U.: Retrieval of microphysical properties of liquid water clouds from atmospheric lidar measurements: Comparison of the Raman dual field of view and the depolarization techniques, Proc. SPIE 10429, 1042907, https://doi.org/10.1117/12.2281806, 2017.

Jimenez, C., Ansmann, A., Donovan, D., Engelmann, R., Schmidt, J., and Wandinger, U.: Comparison between two lidar methods to retrieve microphysical properties of liquid water clouds, EPJ Web Conf., 176, 01032, https://doi.org/10.1051/epjconf/201817601032, 2018.

Jimenez, C., Ansmann, A., Engelmann, R., Malinka, A., Schmidt, J., and Wandinger, U.: Retrieval of microphysical properties of liquid water clouds from atmospheric lidar measurements: dual field of view depolarization technique, Atmos. Meas. Tech. (working paper), 2018b.

Kanitz, T., Seifert, P., Ansmann, A., Engelmann, R., Althausen, Casiccia, C., and Rohwer, E. G.: Contrasting the impact of aerosols at northern and southern midlatitudes on heterogeneous ice formation, Geophys. Res. Lett., 38, L17802, doi:10.1029/2011GL048532, 2011.

Li, J., Jian, B., Huang, J., Hu, Y., and Wu, M.: Long-term variation of cloud droplet number concentrations from space-based Lidar, Rem. Sens. Environment, 213, 144-161, 2018

Liu, B., and Wang, Z.: Improved calibration method for depolarization lidar measurement, Opt. Express, 21, 14583-14590, https://doi.org/10.1364/OE.21.014583, 2013.

Lu, S. Y., and Chipman, R. A.: Interpretation of Mueller matrices based on polar decomposition, J. Opt. Soc. Am. A, 13, 1106–1113, 1996.

Malinka, A.V, and Zege, E.P.: Analytical modeling of Raman lidar return, including multiple scattering, Appl. Optics, 42, 1075-1081, 2003.

Malinka, A. V., and Zege, E. P.: Possibilities of warm cloud microstructure profiling with multiple-field-of-view Raman lidar, Appl. Optics 46, 8419–8427, 2007.

Mamouri, R. E., and Ansmann, A.: Potential of polarization lidar to provide profiles of CCN- and INP-relevant aerosol parameters, Atmos. Chem. Phys., 16, 5905-5931, https://doi.org/10.5194/acp-16-5905-2016, 2016.

Mattis, I., Ansmann, A., Müller, D., Wandinger, U., and Althausen, D.: Multiyear aerosol observations with dualwavelength Raman lidar in the framework of EARLINET, J. Geophys. Res., 109, D13203, doi:10.1029/2004JD004600, 2004.

Mattis, I., Müller, D., Ansmann, A., Wandinger, U., Preißler, J., Seifert, P., and Tesche, M.: Ten years of multiwavelength Raman lidar observations of free-tropospheric aerosol layers over central Europe: Geometrical properties and annual cycle, J. Geophys. Res., 113, D20202, doi:10.1029/2007JD009636, 2008.

Mattis, I., Tesche, M., Grein, M., Freudenthaler, V., and Müller, D.: Systematic error of lidar profiles caused by a polarization-dependent receiver transmission: quantification and error correction scheme, Appl. Optics, 48, 2742-2751, 2009.

Mattis, I., Seifert, P., Müller, D., M. Tesche, Hiebsch, A., Kanitz, T., Schmidt, J., Finger, F., Wandinger, U., and Ansmann, A.: Volcanic aerosol layers observed with multiwavelength Raman lidar over central Europe in 2008–2009, J. Geophys. Res., 115, D00L04, doi:10.1029/2009JD013472, 2010.

McCullough, E. M., Sica, R. J., Drummond, J. R., Nott, G., Perro, C., Thackray, C. P., Hopper, J., Doyle, J., Duck, T. J., and Walker, K. A.: Depolarization calibration and measurements using the CANDAC Rayleigh–Mie–Raman lidar at Eureka, Canada, Atmos. Meas. Tech., 10, 4253-4277, https://doi.org/10.5194/amt-10-4253-2017, 2017.

McCullough, E. M., Sica, R. J., Drummond, J. R., Nott, G. J., Perro, C., and Duck, T. J.: Three-channel single-wavelength lidar depolarization calibration, Atmos. Meas. Tech., 11, 861-879, https://doi.org/10.5194/amt-11-861-2018, 2018.

Okamoto, H., Sato, K., Makino, T., Nishizawa, T., Sugimoto, N., Jin, Y., and Shimuzi, A.: Depolarization ratio of clouds measured by multiple –field of view multiple scattering polarization lidar, EPJ Web Conf., 119, 11007, ILRC 27, https://doi.org/10.1051/epjconf/201611911007, 2016.

Pappalardo, G., Amodeo, A., Apituley, A., Comeron, A., Freudenthaler, V., Linne, H., Ansmann, A., Bösenberg, J., D'Amico, G., Mattis, I., Mona, L., Wandinger, U., Amiridis, V., Alados-Arboledas, L., Nicolae, D., and Wiegner, M.: EARLINET: towards an advanced sustainable European aerosol lidar network, Atmos. Meas. Tech., 7, 2389-2409, doi:10.5194/amt-7-2389-2014, 2014.

Reichardt, J., Baumgart, R., and McGee, T. J.: Three-signal method for accurate measurements of depolarization ratio with lidar, Appl. Opt, 42, 4909-4913, 2003.

Schmidt, J., Wandinger, U., and Malinka, A.: Dual-field-of-view Raman lidar measurements for the retrieval of cloud microphysical properties, Appl. Optics 52, 2235–2247, 2013.

Schmidt, J., Ansmann, A., Bühl, J., Baars, H., Wandinger, U., Müller, D., and Malinka, A. V.: Dual-FOV Raman and Doppler lidar studies of aerosol-cloud interactions: Simultaneous profiling of aerosols, warm-cloud properties, and vertical wind, J. Geophys. Res. Atmos., 119, 5512–5527, 2013b.

Schmidt, J., Ansmann, A., Bühl, J., and Wandinger, U.: Strong aerosol–cloud interaction in altocumulus during updraft periods: lidar observations over central Europe, Atmos. Chem. Phys., 15, 10687-10700, https://doi.org/10.5194/acp-15-10687-2015, 2015.

Sekiguchi, M., Nakajima, T., Suzuki, K., Kawamoto, K., Higurashi, A., Rosenfeld, D., Sano, I., and Mukai, S.: A study of the direct and indirect effects of aerosols using global satellite data sets of aerosol and cloud parameters, J. Geophys. Res., 108(D22), 4699, doi:10.1029/2002JD003359, 2003.

Stelmaszczyk, K., Dell'Aglio, M., Chudzyński, S., Stacewicz, T., and Wöste, L.: Analytical function for lidar geometrical compression form-factor calculations, Appl. Opt., 44, 1323-1331, 2005.

Twomey, S.: Influence of pollution on shortwave albedo of clouds, J. Atmos. Sci., 34, 1149–1152, 1977.